

NASA TECHNICAL NOTE



NASA TN D-5861

C.1

NASA TN D-5861

LOAN COPY: RETURN  
AFWL (WL0L)  
KIRTLAND AFB, TX

DL32621



EXPERIMENTAL INVESTIGATION  
OF MULTIPLE-JET LIQUID INJECTION  
INTO HYPERSONIC FLOW

*by William F. Hinson, Paul B. Gooderum,  
and Dennis M. Bushnell*

*Langley Research Center  
Hampton, Va. 23365*





1. Report No. NASA TN D-5861	2. Government Accession No.	3. Recipient's 0132621
4. Title and Subtitle EXPERIMENTAL INVESTIGATION OF MULTIPLE-JET LIQUID INJECTION INTO HYPERSONIC FLOW	5. Report Date June 1970	6. Performing Organization Code
7. Author(s) William F. Hinson, Paul B. Gooderum, and Dennis M. Bushnell	8. Performing Organization Report No. L-6917	10. Work Unit No. 730-00-01-01
9. Performing Organization Name and Address NASA Langley Research Center Hampton, Va. 23365	11. Contract or Grant No.	13. Type of Report and Period Covered Technical Note
12. Sponsoring Agency Name and Address National Aeronautics and Space Administration Washington, D.C. 20546	14. Sponsoring Agency Code	15. Supplementary Notes
16. Abstract Experimental data are presented for liquid injection through three inline orifices 0.051 cm in diameter. The liquid was injected from a flat plate at various downstream angles relative to the free-stream flow. Injection tests were made with different injection-angle combinations at various liquid and tunnel pressures. Free-stream Mach number, depending upon tunnel conditions, varied from 7.80 to 7.95. Some injection data were obtained with three formulations of a fluorocarbon liquid. The results indicate increased penetration when a jet is located in the wake of another jet. A decrease in penetration and in lateral spreading results when the injection angle is rotated downstream from a perpendicular to the surface. The limited data of the fluorocarbon liquid injection indicate that water penetrates farther than the fluorocarbons at the same test conditions.		
17. Key Words (Suggested by Author(s)) Water injection Hypersonic Mach number Penetration	18. Distribution Statement Unclassified - Unlimited	
19. Security Classif. (of this report) Unclassified	20. Security Classif. (of this page) Unclassified	21. No. of Pages 40
		22. Price* \$3.00

# EXPERIMENTAL INVESTIGATION OF MULTIPLE-JET LIQUID INJECTION INTO HYPERSONIC FLOW

By William F. Hinson, Paul B. Gooderum,  
and Dennis M. Bushnell  
Langley Research Center

## SUMMARY

Experimental data are presented for liquid injection through three inline orifices 0.051 cm in diameter. The liquid was injected from a flat plate at various downstream angles relative to the free-stream flow. Injection tests were made with different injection-angle combinations at various liquid and tunnel pressures. Free-stream Mach number, depending upon tunnel conditions, varied from 7.80 to 7.95. Some injection data were obtained with three formulations of a fluorocarbon liquid. The results indicate increased penetration when a jet is located in the wake of another jet. A decrease in penetration and in lateral spreading results when the injection angle is rotated downstream from a perpendicular to the surface. The limited data of the fluorocarbon liquid injection indicate that water penetrates farther than the fluorocarbons at the same test conditions.

## INTRODUCTION

Spacecraft which utilize atmospheric braking during entry into a planetary atmosphere generally experience radio blackout. A program called Project RAM (Radio Attenuation Measurements) is being conducted at the Langley Research Center to obtain a better knowledge and understanding of conditions within the flow field which influence the transmissibility of electromagnetic waves through the plasma around the spacecraft. Techniques for improving communications through such a flow field are continually being developed and evaluated.

To date six flight experiments have been conducted in the RAM program: four at 5486 m/sec and two at 7620 m/sec. The spacecraft geometry was a hemisphere followed by a 90° half-angle conical frustum. One flight at each entry velocity incorporated water injection into the flow field about the spacecraft during loss of telemetry signal due to an ionized flow field. Results of these flight experiments are presented in references 1 and 2. Although complete signal recovery at all test conditions was not attained, the two

flight experiments and also the Gemini III mission reported in reference 3 demonstrated that water injection was somewhat effective in reducing electron concentrations in ionized flow fields. Flight data of reference 2 indicated that the ionized flow field was probably thicker than preflight predictions, and that the water was not efficiently distributed through the attenuating layer or layers of plasma. It is also possible that the water-injection parameters such as mass flow, number of orifices, orifice pattern, flow-field penetration, and distribution were not optimized. The technique used in the flight of reference 2 consisted of injecting water through two to 14 nozzles emanating from and perpendicular to the spacecraft surface at approximately the tangency point between the hemisphere and cone. The nozzle arrangements were similar to a "bowling pin" pattern. Prior to the flight a wind-tunnel program was conducted to study the penetration characteristics of the water-injection technique. The results of the experimental program are presented in reference 4.

Another RAM-C flight, RAM C-C, is planned at the 7620 m/sec entry velocity. The experiment requires that water and fluorocarbon be injected into the flow field from approximately the tangency point between the hemisphere and cone. The liquid-injection technique proposed for this flight is markedly different from the technique used on the earlier flight. The proposed changes were based on flight-data analysis mentioned previously and the experimental data of reference 4. In reference 4 the schlieren photographs show that when the required maximum penetration of water was obtained downstream the initial penetration at the injection site was sufficient to cause significant bow-shock disturbance. The bow-shock disturbance would result in increased ion production in the flow field about the spacecraft. Therefore, in order not to disturb the bow shock in the RAM C-C flight, the angle of liquid injection has been rotated downstream; the choice of angle is discussed herein. The multiple-orifice injection data of reference 4 also indicated a penetration increase when an orifice was shielded by the wake of another orifice. Therefore, the orifice arrangement proposed for RAM C-C is a rectangular pattern of longitudinal rows to take advantage of the shielding effect.

The problem of predicting penetration and/or distribution of a liquid into supersonic and hypersonic streams has been studied for many years. (For example, see refs. 5 to 8.) Most of the data are for single-orifice injection normal to a surface or for stagnation-point injection. In reference 7 experimental data are presented for a single jet emanating from a flat surface at various upstream, normal, and downstream angles relative to the surface. The conclusion is made that maximum penetration downstream of the injection site is obtained by injecting upstream at an angle between  $35^{\circ}$  and  $55^{\circ}$  measured from a perpendicular to the injection surface. In reference 8 data are presented for forward injection and the conclusion contradicts the conclusions of reference 7. Also in this reference limited data are presented for a dual orifice arrangement which is similar to the

orifice shielding arrangement presented in reference 4. The conclusions of reference 8 state that almost no increase in penetration is attained with a shielded jet; this conclusion contradicts the data presented in reference 4.

From these references, then, it is very difficult to establish trends and penetration prediction methods to define a complete injection system such as proposed for the RAM C-C flight. Therefore, an extensive wind-tunnel program similar to that reported in reference 4 was formulated to generate experimental data with scaled models of the RAM C-C spacecraft and injection system. To aid in the planning of this program and to establish design limits, a wind-tunnel program of an exploratory nature was conducted in the Langley Mach 8 variable-density tunnel. The model was a flat plate with a row of three orifices similar to a row of orifices proposed for the RAM C-C flight. Three areas were explored: (1) shielding effect of the lead orifice, (2) orifice injection angle relative to the flat-plate surface, and (3) comparison of the injection characteristics of three types of fluorocarbon liquids with those of water. The purpose of this paper is to present the results of the exploratory program.

#### SYMBOLS

p	pressure
V	velocity
x	downstream distance from injection site
y	spray height above flat plate
z	lateral spreading of liquid spray
$\rho$	density
$\frac{\rho_j V_j^2}{\rho_L V_L^2}$	dynamic-pressure ratio
Subscripts:	
j	water jet before breakup
L	local airflow conditions at injection site

$l$	liquid
$t$	tunnel total condition

## APPARATUS AND TEST METHODS

### Tunnel

The investigation was conducted in the Langley Mach 8 variable-density tunnel. This tunnel is of the blowdown type and has an axially symmetric nozzle with contoured walls. For the present tests the total pressure  $p_t$  was varied from 1.72 MN/m<sup>2</sup> (17 atm) to 17.23 MN/m<sup>2</sup> (170 atm). The corresponding free-stream Mach number range was 7.80 to 7.95. The free-stream static-pressure range was from 200 N/m<sup>2</sup> (0.002 atm) to 1900 N/m<sup>2</sup> (0.018 atm). For the present tests the stagnation temperature varied from approximately 722<sup>o</sup> to 811<sup>o</sup> K. The facility is described more fully in reference 9.

### Flat Plate

A sketch of the stainless-steel flat plate used in the investigation is shown in figure 1. The leading edge was machined to a thickness of approximately 0.013 cm. The plate was constructed to receive a threaded plug. Each interchangeable plug contained three orifices. A plenum chamber was installed on the lower side of the plate underneath the orifice-plug receptacle. This chamber was connected to the liquid-injectant supply system, which was a series of storage tanks pressurized to the desired level by gaseous nitrogen. A pressure transducer and thermocouple monitored the pressure and temperature of the fluid in the plenum chamber, which was shielded from exposure to the high-temperature free-stream flow. Liquid pressure  $p_l$  was varied from about 0.45 MN/m<sup>2</sup> (4.4 atm) to 3.52 MN/m<sup>2</sup> (35 atm). The plate was set at an angle of attack of approximately 1<sup>o</sup> in order to adjust the static pressure on the plate center line to near free-stream static pressure.

### Orifice Configurations

Sketches of the orifice configurations tested are shown in figure 2. Each configuration consists of three orifices 0.051 cm in diameter and approximately 0.5 cm apart. The injection angle relative to a perpendicular to the injection surface was varied from 9<sup>o</sup> to 39<sup>o</sup> downstream. The exit cross sections taken parallel to the plate surface of configurations 1 to 4 were elliptical, the ellipticity depending upon the injection angle of the orifice. The orifice exits of configuration 5 were counterbored to achieve circular exit cross sections. Individual calibration of the orifices of each configuration yielded an overall

discharge coefficient of approximately 0.70. The orifice plug and the plate were carefully alined to insure that the center line of the three orifices was parallel to the free-stream flow.

### Photographic Observation Equipment

The location of the photographic equipment with respect to the tunnel test section is shown in figure 3. Penetration and lateral spreading of the liquid spray into the flow field above the flat plate were observed by means of two cameras and two light sources. The two camera-light combinations were operated independently.

For the light-screen photograph an intense light was oriented so as to illuminate the liquid-spray penetration in the vertical plane parallel to the free-stream flow from the injection site to about 22 cm downstream. The light source and camera were mounted on about the same horizontal plane as the flat plate. Prior to the investigation a photograph was made of a grid card which was placed on the center line perpendicular to the flat plate to establish a measuring system for the liquid-spray penetration. The camera was mounted rigidly and was not moved during the test. A schematic of the light-screen photograph image and the flat plate is shown in figure 3(b).

Lateral spreading of the liquid spray was observed by means of a beam light source directed through the test section so as to illuminate a cross section of the liquid spray in the vertical plane perpendicular to the free-stream flow at approximately 16 cm from the injection site. A photograph of a grid card at this position and orientation was made prior to the investigation to establish a measuring system. The camera viewing the lateral spreading was mounted slightly above the plate to provide a three-dimensional image. A schematic of the plate and the photographic image is presented in figure 3(c).

A conventional single-pass schlieren system with parabolic mirrors 45.72 cm in diameter having a focal length of 233.68 cm was used to view the liquid spray and associated flow-field phenomena. Representative schlieren photographs of water injection are presented in figure 4.

## RESULTS AND DISCUSSION

### General

The schlieren photographs show that weak expansion and shock waves exist at the plate leading edge and in the vicinity of the injection site. Also, some flow separation is evident on the plate. However, the thickness of the separated layer is small compared with the overall penetration of the liquid spray. The static pressure on the plate near the injection site was near free-stream static pressure and in the schlieren photographs

the weak expansion and shock waves and the flow separation do not appear to be causing interference with the liquid spray; therefore, it is believed that for the purpose of the present investigation the flow over the plate in the injection region was of an acceptable quality.

Ice formation on the plate at tunnel total pressures of  $3.45 \text{ MN/m}^2$  and above was practically nonexistent. Two light-screen photographs of water at a tunnel total pressure of  $3.45$  and  $1.72 \text{ MN/m}^2$  indicate some ice on the plate (figs. 9(b) and 9(c)); however, the liquid penetration does not appear to be affected.

The schlieren photographs show that the jet of liquid, after emanating from the plate surface, remains a relatively solid stream for a distance and then disintegrates into a spray. Thus, in the light-screen photographs the spray is illuminated and extends from the plate surface out to some maximum distance. Measurements of the outer edge of the illuminated spray were made from the light-screen photographs and are plotted as maximum penetration  $y$  against downstream location  $x$ . The photographs and measured data are presented in figures 5 to 9. The origin of the  $x,y$  plot is taken as the center line of the lead orifice. (See fig. 3(c).) These light-screen photographs and measured data indicate that various penetration heights can be achieved by varying liquid pressure at constant tunnel pressure or by constant liquid pressure and varying tunnel pressure. The dashed lines shown in the plotted spray trajectories indicate the relationship of the jet pattern and angle of injection. The "humps" in the initial part of the trajectory are the result of "jet shielding," which is discussed in the following paragraph.

#### Orifice Shielding Effect

In reference 4 it is shown that when one jet shields another the solid and spray portions of the shielded jet penetrate farther into the flow field. In the present investigation, increased penetration due to shielding is shown by the light-screen photographs and measured spray-trajectory comparisons of 1-, 2-, and 3-orifice operations in figures 5(a), 6(a), 7(a), and 8(a). Evidently the initial jet acts as a quasi-solid cylindrical body producing a wake which is characterized by low dynamic pressure. The second jet acts in a like manner to produce another wake of different conditions to which the third jet is subjected. The relative lengths of the solid jets in the multijet operation could not be measured from the schlieren photographs in reference 4 or in the present study because of density variations. In the present investigation, the relative lengths of the solid jets were determined by direct visual means and also by using a closed-circuit television camera. From these observations of the solid jet lengths for all the configurations investigated, it was found that the first shielded jet penetrated about twice as far as the shielding jet and the third jet in line or the second shielded jet penetrated about three times as far as the first jet. This relationship does not hold true for the maximum penetration downstream,

that is, where the maximum height of the spray becomes approximately parallel to the plate surface at about 20 cm from the injection location. At this location, maximum penetration of the individual jets appears to be a function of the injection-angle combination, which is discussed in the following paragraph.

### Effect of Orifice Injection Angle

For single-orifice injection, as the injection angle is rotated downstream from  $9^\circ$  to  $39^\circ$  the maximum penetration of the liquid spray is decreased at any given x-dimension. (See figs. 5(a), 6(a) or 7(a), and 8(a).) This result agrees with the data presented in reference 7 and is expected since the component of momentum of the liquid jet perpendicular to the free stream is decreased as the angle of injection is rotated downstream. The second orifice or first shielded orifice also shows a decrease in penetration as its injection angle is rotated downstream from  $9^\circ$  to  $39^\circ$  (figs. 5(a), 6(a), and 8(a)). At  $x = 20$  cm the penetration decrease is about one-half that of the lead or shielding orifice. The third jet appears to be affected by the injection-angle combination since the third jets of figures 6(a), 7(a), and 8(a), all injecting at  $39^\circ$  downstream and shielded, do not penetrate the same. When the jets are all parallel, as in figure 8(a), the third jet penetrates farther. In the aforementioned direct visual and television observation the outer edge of the liquid appeared very steady at a particular tunnel and injection-pressure condition. Therefore, the effects of shielding and angle of injection on maximum penetration seem to be dependent on the particular combination of angles in a particular orifice configuration and also the wake characteristics of that particular configuration.

### Fluorocarbon Injection

Three types of fluorocarbon liquid were used with configuration 5 (fig. 2) in a limited number of injection tests. Some pertinent physical properties of the fluorocarbons and of water are listed in table I. These physical properties were obtained from reference 10 and other data sources and calculations related to that reference. Results of the fluorocarbon injection tests are presented in figure 9. In these tests the liquid pressure was kept constant while the tunnel stagnation pressure was varied.

In general, the results with fluorocarbon injection were very similar to those with water injection. At the same test conditions, the water penetrated farther into the flow field. Some small differences in maximum penetration of the various types of fluorocarbon are noted. Apparently the greater density of the fluorocarbons results in a decrease in liquid velocity which decreases the penetration. Another possibility is that, because of the lower heat of vaporization of the fluorocarbons, increased vaporization could have occurred, resulting in lower penetration as detected by the photographic technique.

The relative evaporative lifetime of the atomized mean droplets of the fluorocarbons is 2 orders of magnitude less than that of water. (See table I.) Therefore, it appears possible that the photographic technique could not detect the complete penetration of the fluorocarbon.

The orifice modification of configuration 5 had little effect on the maximum spray penetration of water at  $x = 20$  cm, as can be seen by comparing figures 8(c) and 8(d) with figures 9(a) and 9(b) at similar test conditions.

### Relative Lateral Spreading and Penetration

Relative lateral spreading and penetration with water as the injectant are shown by the light images on the black background in figures 10 and 11. These images represent the spray cross section at approximately 16 cm from the injection site. (See fig. 3(c).) Liquid and free-stream flow is from right to left. The upper surface of the plate is represented by the  $x,z$  plane, the  $x$ -axis being the plate center line which extends through the center of the inline injection orifices. The  $y,z$  plane is perpendicular to the plate. Lateral spreading is along the  $z$ -axis and is symmetrical about the  $y$ -axis. Because of the camera viewing angle, the  $y,z$  plane, which includes the spray cross-sectional image, appears to be skewed relative to the free-stream flow. Measurements of the relative lateral spreading and penetration in the  $y,z$  plane can be obtained directly by the use of the grid scale provided on the figures. The greater width at the bottom of the spray image is believed to be the result of spreading within the previously mentioned separated flow region on the plate or light reflections from the plate causing a double image. Only the upper portion of the spray image, as labeled in figure 10, will be considered in the following discussion. Only one photograph is labeled since all other photographs are similar.

In figure 10 typical photographs are presented to show the relative lateral spreading and penetration of 1-, 2-, and 3-orifice injections from orifice configurations 1, 2, and 4. (See fig. 2.) For each orifice configuration the photographs show that lateral spreading and penetration increase with the number of orifices injecting. Comparisons of the dual- and triple-injection photographs of orifice configurations 1 and 4 indicate that as the angle of injection is rotated downstream from  $9^\circ$  to  $39^\circ$  the lateral spreading and penetration decrease.

The photographs of figure 11 show that lateral spreading and penetration increase with increasing liquid pressure at constant tunnel total pressure  $p_t$ . At constant liquid injection pressure, decreasing tunnel total pressure results in increases in liquid penetration but the lateral spreading remains nearly constant.

## Penetration Correlation

In references 4 and 7 it has been shown that the parameter which influences the behavior of a coherent jet in its initial state (very near the injection site) is the square root of the dynamic-pressure ratio at the injection site. Figure 12 shows the maximum liquid spray penetration  $y$  for each orifice configuration as a function of this parameter. The curves indicate a good correlation for each orifice configuration (3-orifice operation), even though the maximum penetration at a particular test condition has been shown to vary with injection angle and injection-angle combination. Also shown in the figure is the maximum spray penetration for single- and double-jet operation. The effect of jet shielding is readily observed since the penetration of the shielded third jet varies up to about twice that for no shielding (single-orifice injection).

## SUMMARY OF RESULTS

Experimental data are presented for liquid injection through three inline orifices 0.051 cm in diameter. The liquid was injected from a flat plate at various downstream angles relative to the free-stream flow. Water was injected with different angle combinations at various liquid and tunnel pressures. Also, limited injection data were obtained with three formulations of fluorocarbon liquid.

A decrease in penetration and lateral spreading resulted when the injection angle was rotated downstream from a perpendicular to the plate. Increased penetration resulted when a jet was shielded or located in the wake of another jet. In a limited investigation at constant tunnel pressure and liquid pressure and with the same orifice configuration, water penetrated farther into the flow field than the three formulations of fluorocarbon. The three formulations of fluorocarbon had almost the same injection characteristics. The square root of the local dynamic-pressure ratio is shown to correlate the maximum water-spray penetration of each orifice configuration.

Langley Research Center,  
National Aeronautics and Space Administration,  
Hampton, Va., April 24, 1970.

## REFERENCES

1. Cuddihy, William F.; Beckwith, Ivan E.; and Schroeder, Lyle C.: RAM B2 Flight Test of a Method for Reducing Radio Attenuation During Hypersonic Reentry. NASA TM X-902, 1963.
2. Akey, Norman D.; and Cross, Aubrey E. (With appendix A by Thomas G. Campbell, appendix B by Fred B. Beck, and appendix C by W. Linwood Jones, Jr.): Radio Blackout Alleviation and Plasma Diagnostic Results From a 25 000 Foot Per Second Blunt-Body Reentry. NASA TN D-5615, 1970.
3. Schroeder, Lyle C.: Gemini Reentry Communications Experiment. NASA paper presented at the Third Symposium on Plasma Sheath (Boston, Mass.), Sept. 23, 1965.
4. Weaver, William L.; and Hinson, William F.: Water Injection From a 9° Hemisphere-Cone Into a Hypersonic Airstream. NASA TN D-5739, 1970.
5. Beckwith, Ivan E.; Bushnell, Dennis M.; and Huffman, Jarrett K.: Investigation of Water Injection of Models of Gemini Vehicle and Resulting Predictions for GT-3 Reentry Communications Experiment. NASA TM X-1200, 1966.
6. Bushnell, Dennis M.; and Huffman, Jarrett K.: Forward Penetration of Liquid Water and Liquid Nitrogen Injected From an Orifice at the Stagnation Point of a Hemispherically Blunted Body in Hypersonic Flow. NASA TM X-1493, 1968.
7. Catton, I.; Hill, D. E.; and McRae, R. P.: Study of Liquid Jet Penetration in a Hypersonic Stream. AIAA J., vol. 6, no. 11, Nov. 1968, pp. 2084-2089.
8. Kolpin, M. A.; Horn, K. P.; and Reichenbach, R. E.: Study of Penetration of a Liquid Injectant Into a Supersonic Flow. AIAA J., vol. 6, no. 5, May 1968, pp. 853-858.
9. Schaefer, William T., Jr.: Characteristics of Major Active Wind Tunnels at the Langley Research Center. NASA TM X-1130, 1965.
10. Kurzius, Shelby C.; and Raab, Fredrik H.: Vaporization and Decomposition Kinetics of Candidate Re-Entry Blackout Suppressants in Low Pressure Flames. NASA CR-1330, 1969.

TABLE I.- FLUID PROPERTIES AT 25° C

Fluid	Density, g/cm <sup>3</sup>	Vapor pressure, torr	Viscosity, cP	Surface tension (in air), dyn/cm	Heat of vaporization, cal/g	Relative atomized mean droplet size	Relative evaporative lifetime of atomized mean droplet size
Water	0.997	23.8	0.894	72.0	540	1	1
$F(C_3F_6O)_3CFHCF_3$	1.79	0.2	7.0	15.9	11.0	0.46	0.017
$(C_4F_9)_3N$	1.88	0.3	4.9	16.0	16.7	0.45	0.026
$C_8F_{18}$	1.77	30.0	1.45	14.8	21.1	0.45	0.031

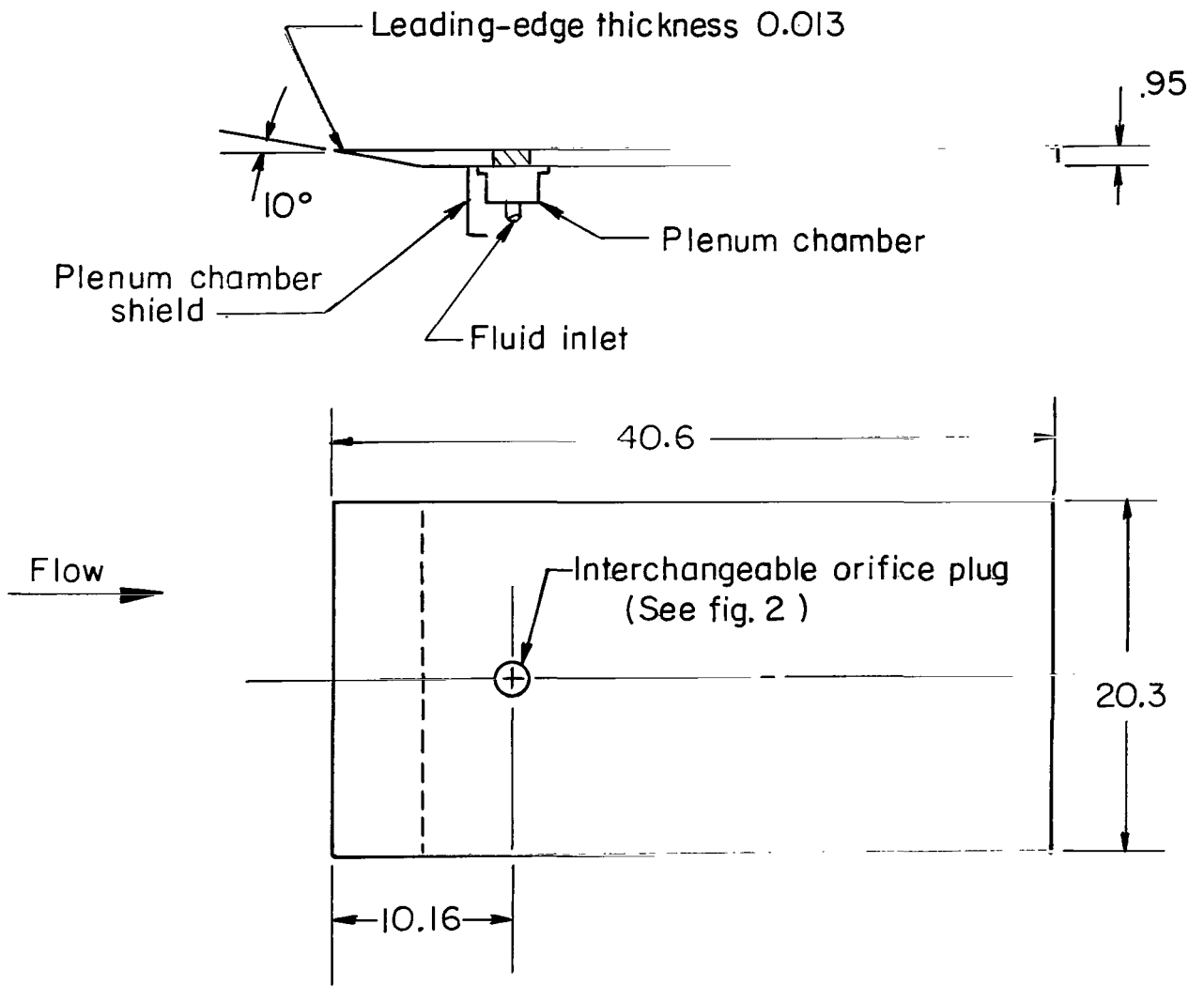


Figure 1.- Schematic of flat plate. All dimensions are in centimeters.

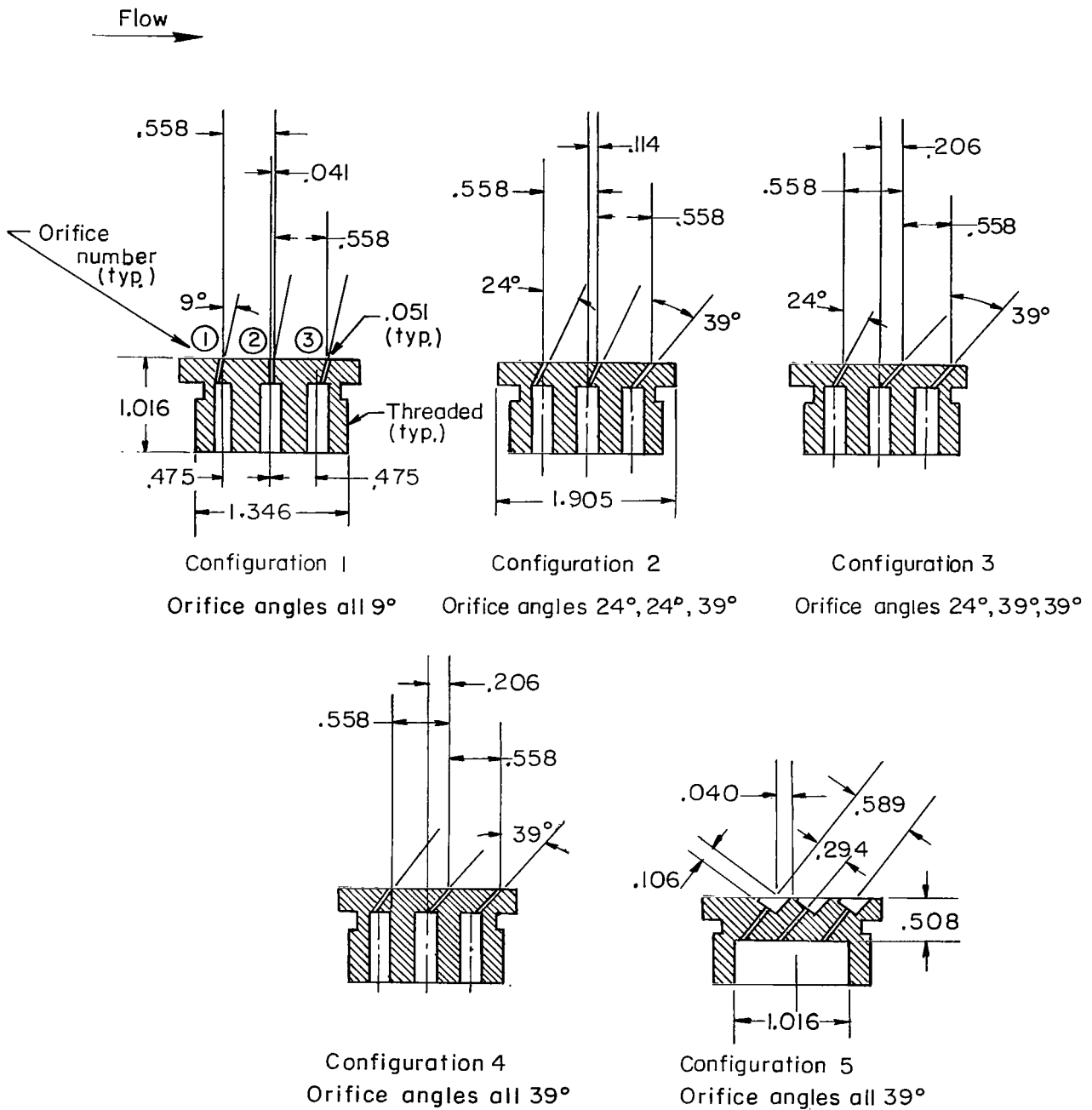
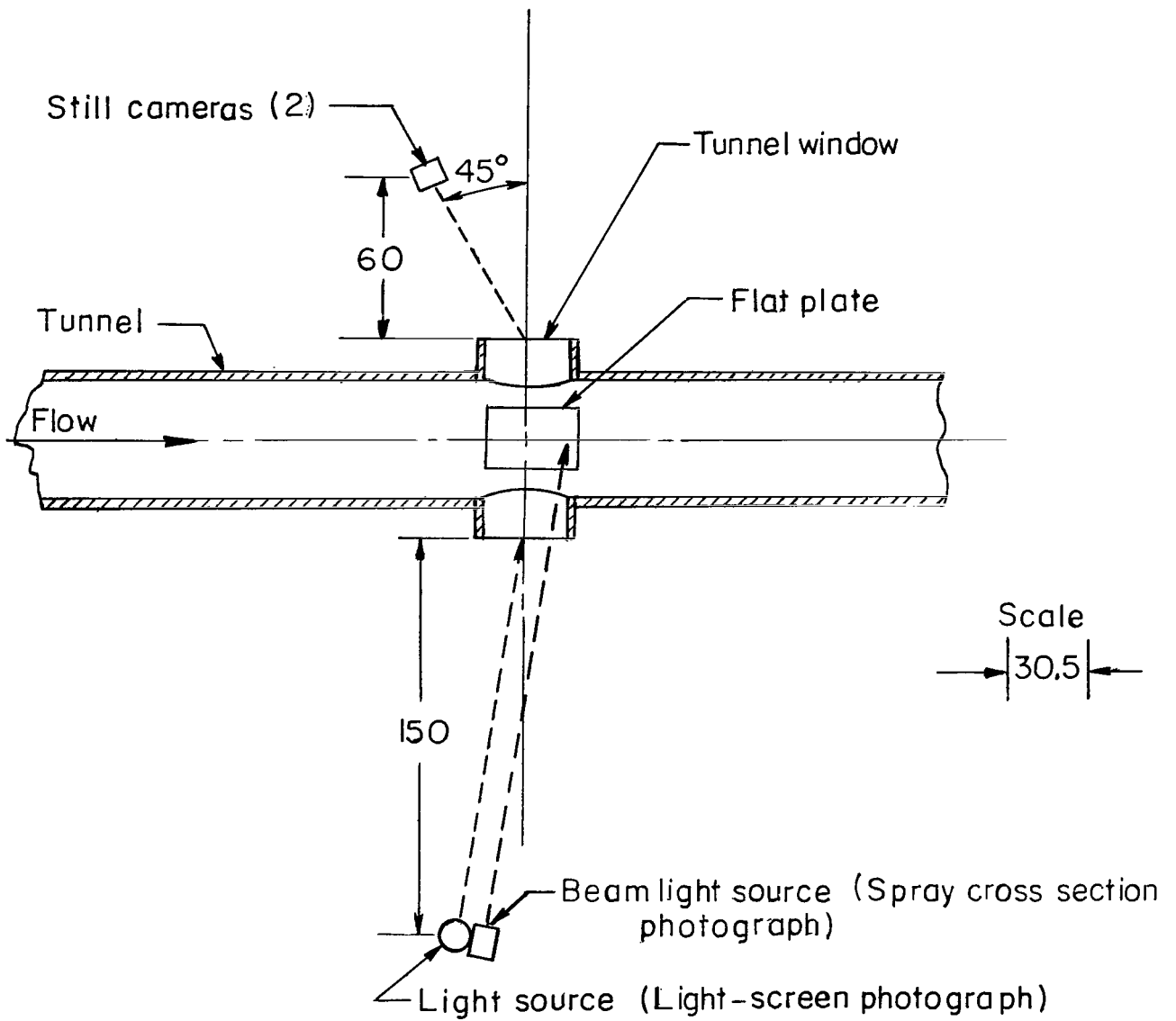
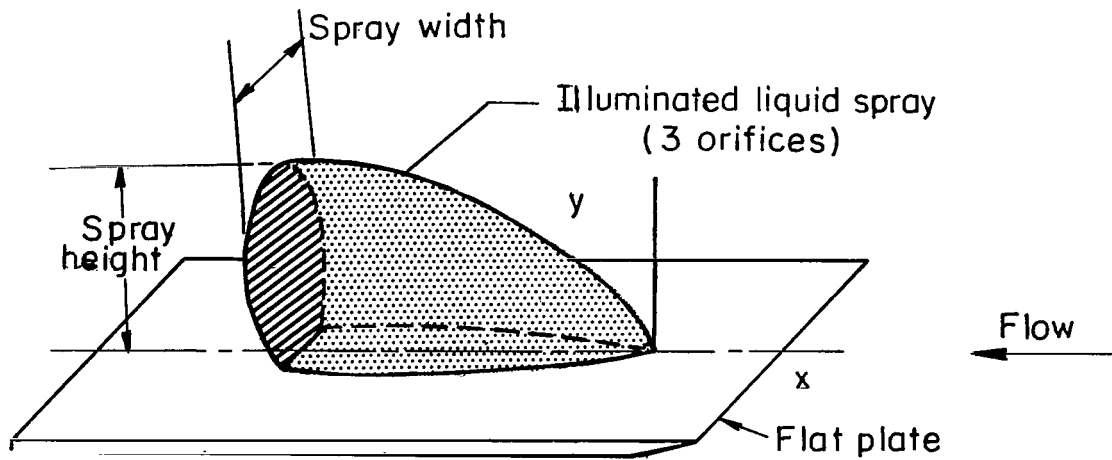


Figure 2.- Orifice configurations tested. All dimensions are in centimeters.

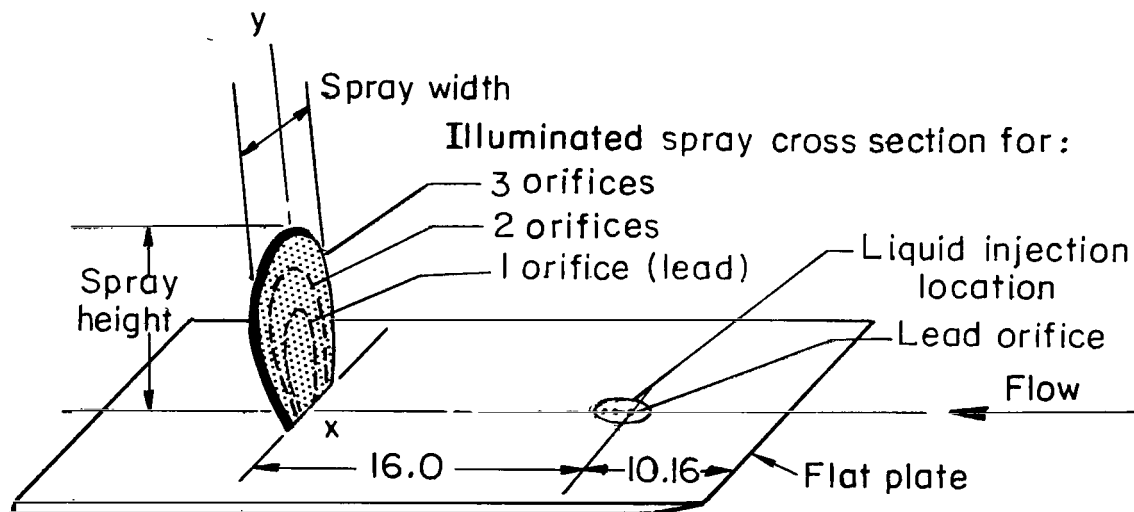


(a) General setup (top view).

Figure 3.- Approximate locations of light sources and cameras. All dimensions are in centimeters.



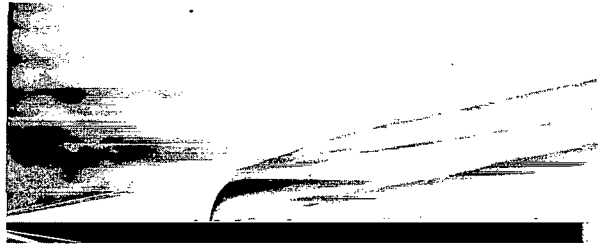
(b) Light-screen photographic schematic.



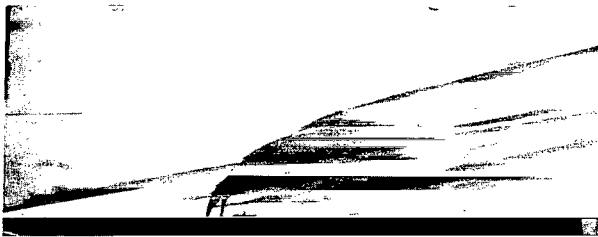
(c) Spray cross-section photographic schematic.

Figure 3.- Concluded.

Flow →



1 orifice



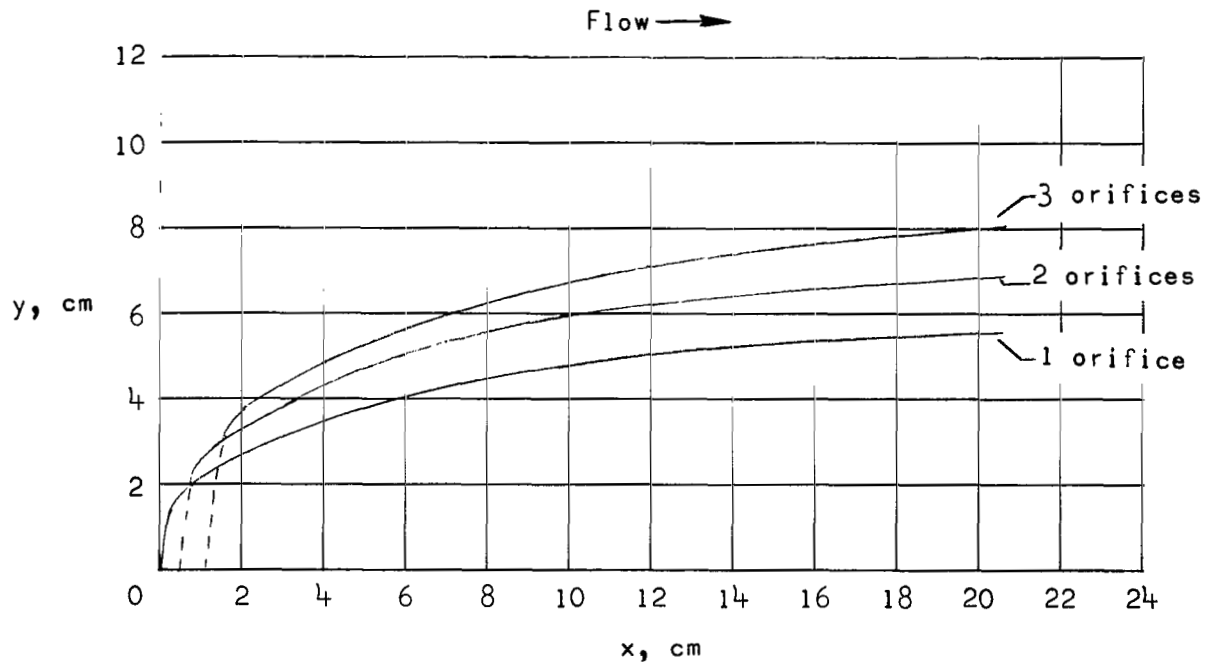
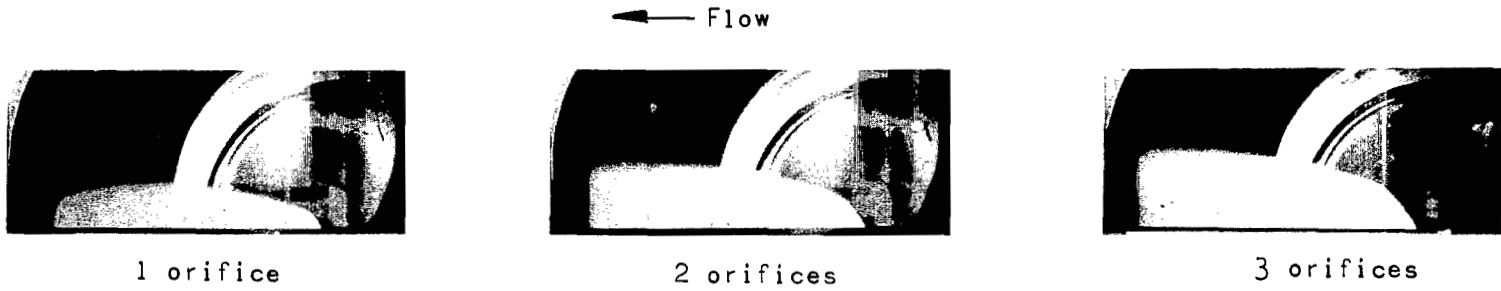
2 orifices



3 orifices

L-70-1601

Figure 4.- Schlieren photographs showing effect of injection through 1, 2, and 3 inline orifices of configuration 1.  
 $p_t = 3.52 \text{ MN/m}^2$ ;  $p_t = 6.89 \text{ MN/m}^2$ .



(a)  $p_t = 3.52 \text{ MN/m}^2$ ;  $p_t = 6.89 \text{ MN/m}^2$ .

L-70-1602

Figure 5.- Light-screen photographs and measured outer limit of water spray trajectories for orifice configuration 1.

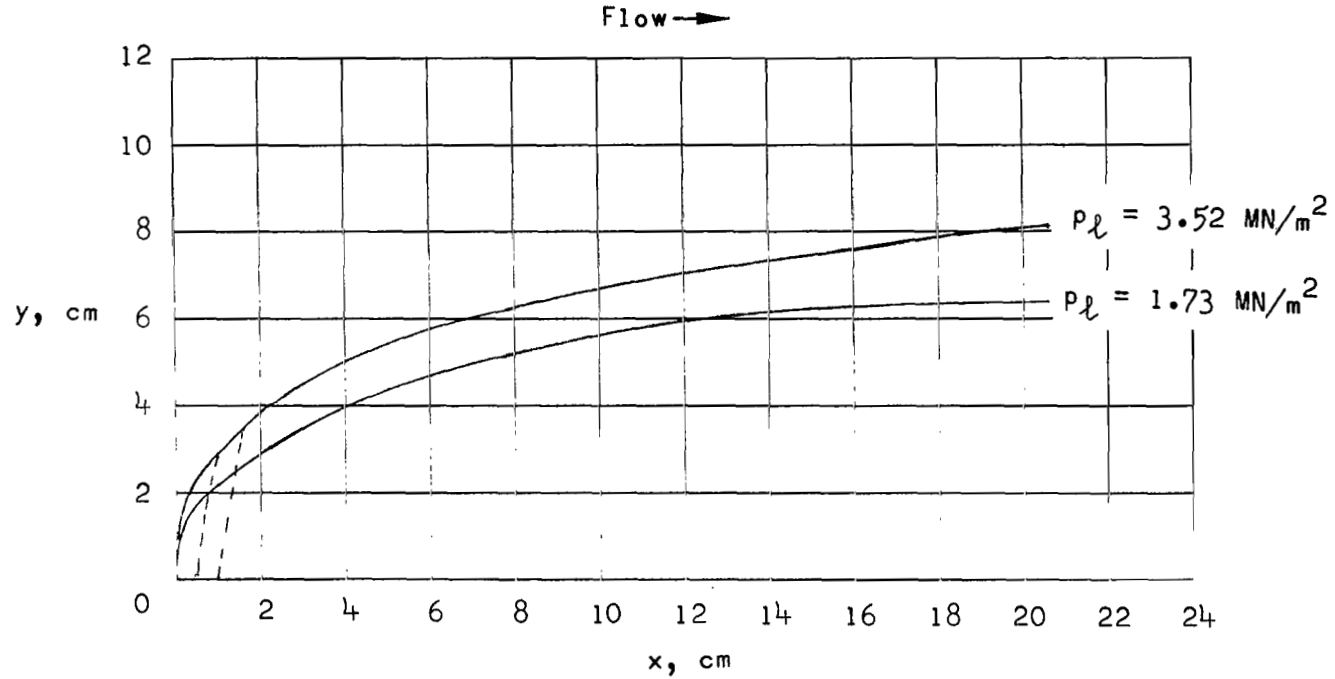
← Flow



$$p_l = 1.73 \text{ MN/m}^2$$



$$p_l = 3.52 \text{ MN/m}^2$$



(b)  $p_t = 6.89 \text{ MN/m}^2$ ; 3 orifices.

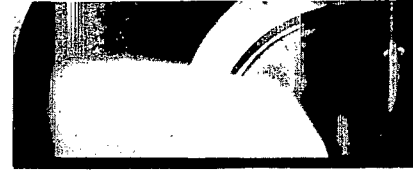
L-70-1603

Figure 5.- Continued.

← Flow

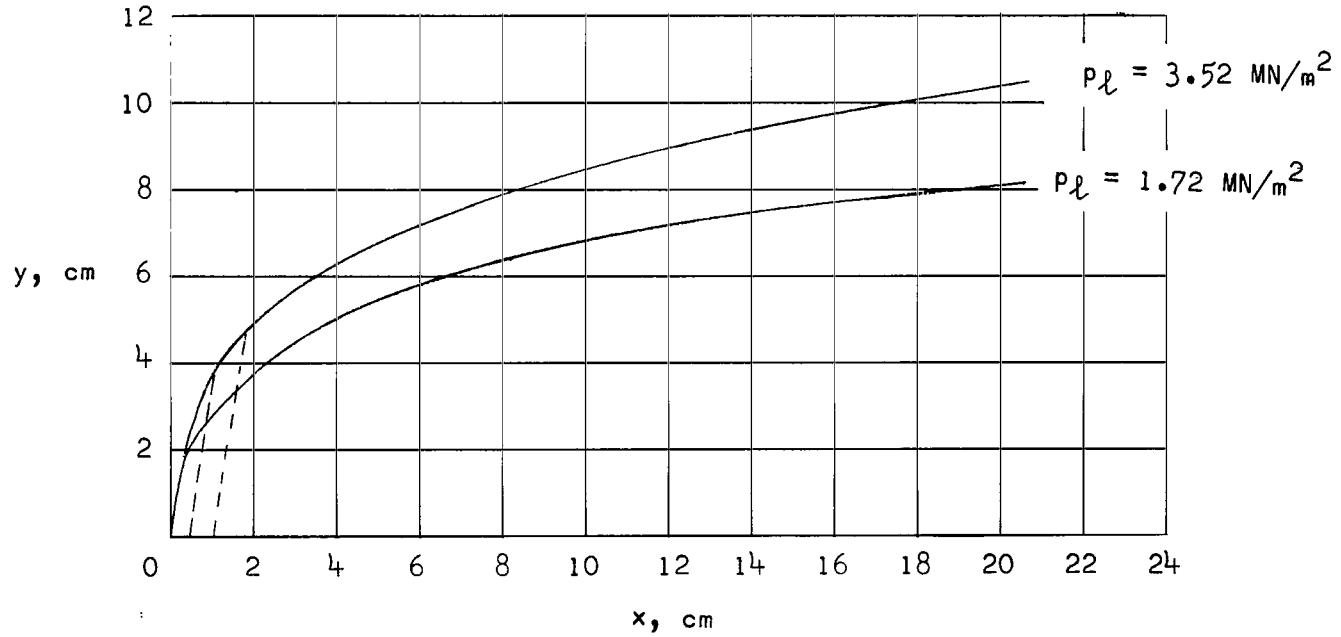


$$p_l = 1.72 \text{ MN/m}^2$$



$$p_l = 3.52 \text{ MN/m}^2$$

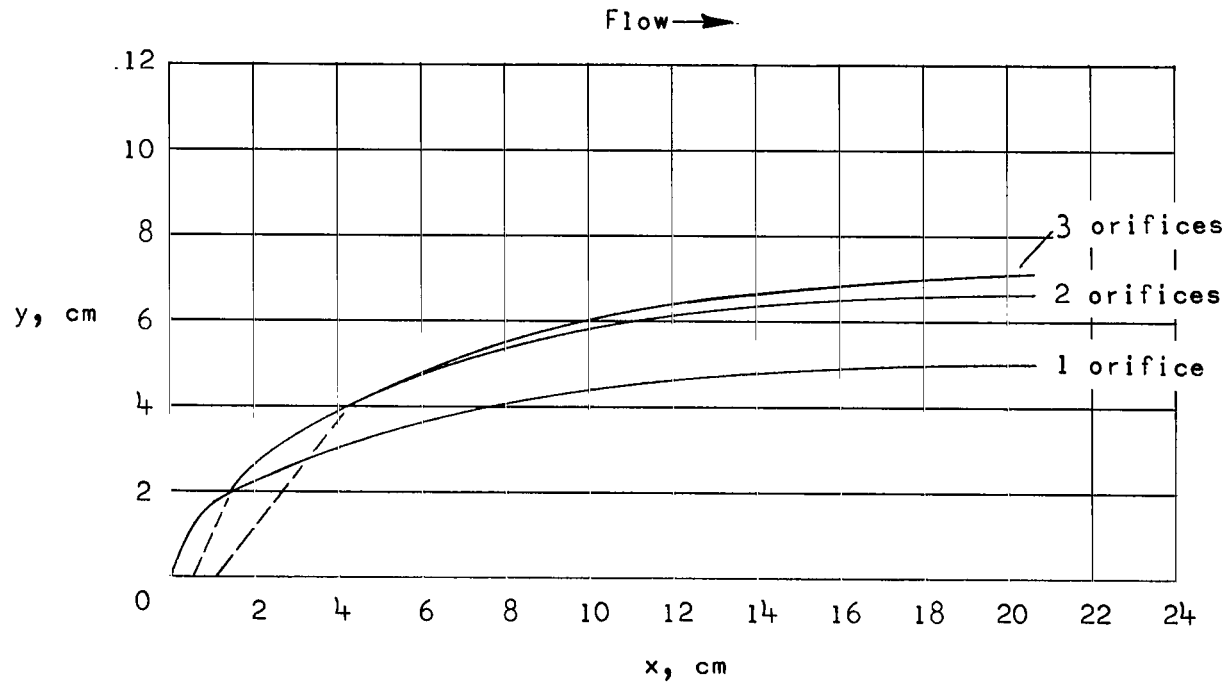
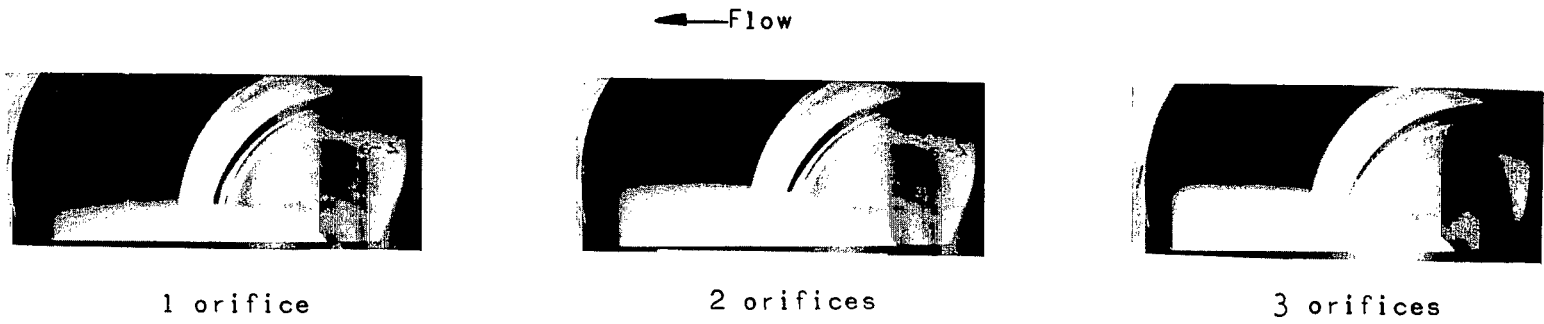
Flow →



(c)  $p_t = 3.44 \text{ MN/m}^2$ ; 3 orifices.

L-70-1604

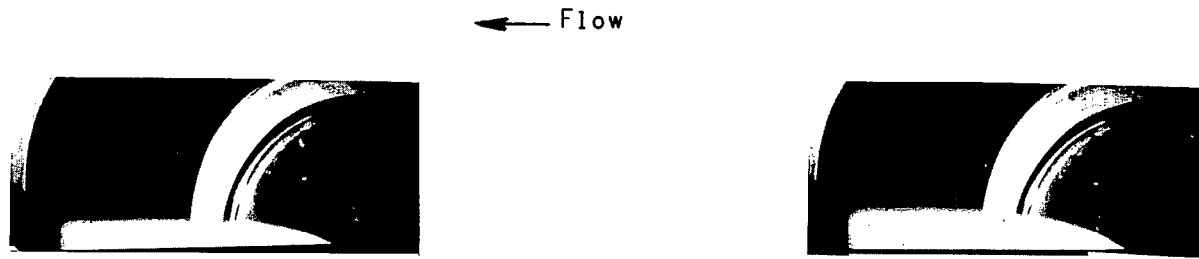
Figure 5.- Concluded.



(a)  $p_t = 3.52 \text{ MN/m}^2$ ;  $p_t = 6.89 \text{ MN/m}^2$ .

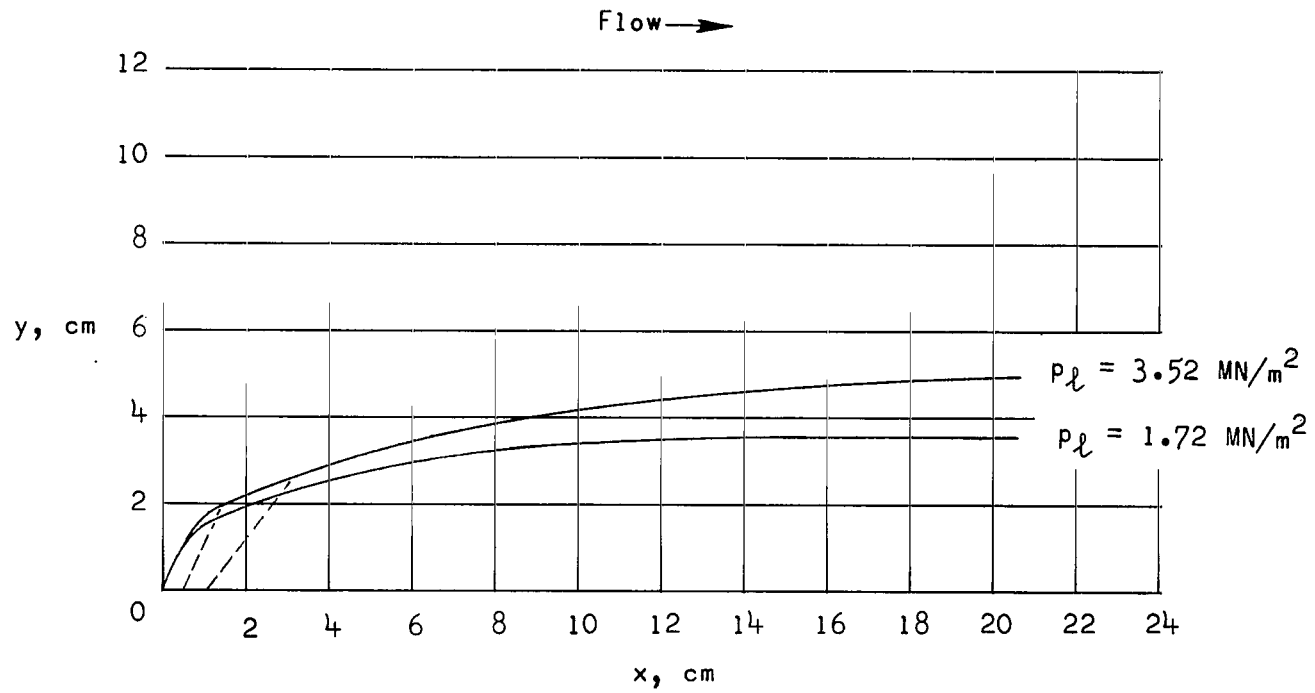
L-70-1605

Figure 6.- Light-screen photographs and measured outer limit of water spray trajectories for orifice configuration 2.



$$p_l = 1.72 \text{ MN/m}^2$$

$$p_l = 3.52 \text{ MN/m}^2$$



(b)  $p_t = 17.23 \text{ MN/m}^2$ ; 3 orifices.

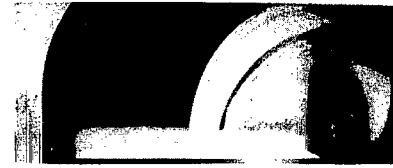
L-70-1606

Figure 6.- Continued.

← Flow



$$P_d = 0.24 \text{ MN/m}^2$$



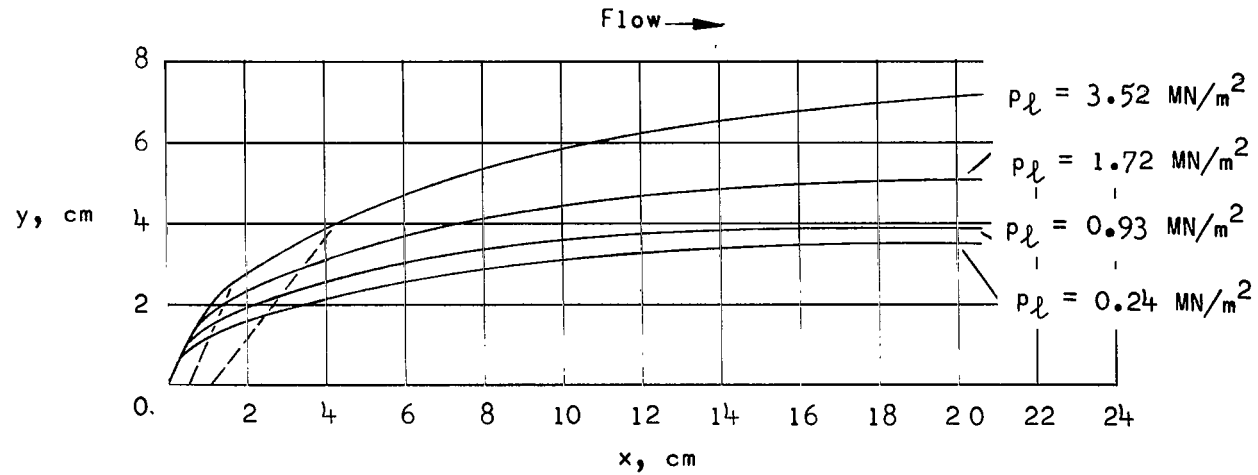
$$P_d = 0.93 \text{ MN/m}^2$$



$$P_d = 1.72 \text{ MN/m}^2$$



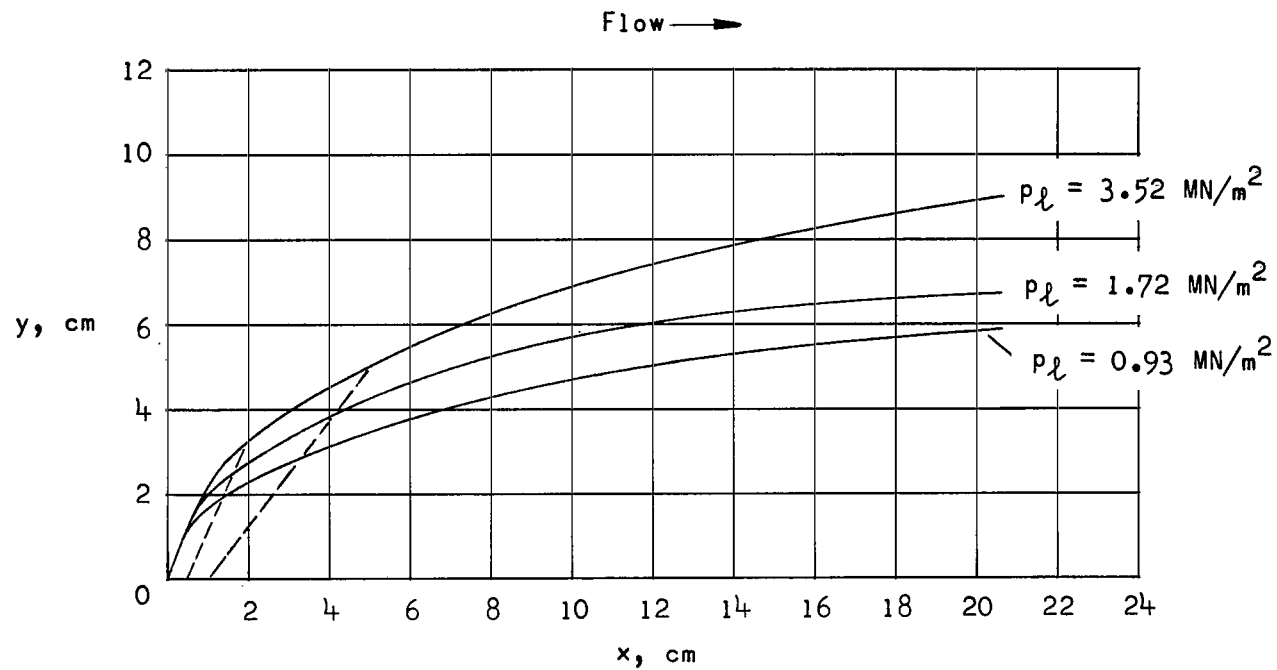
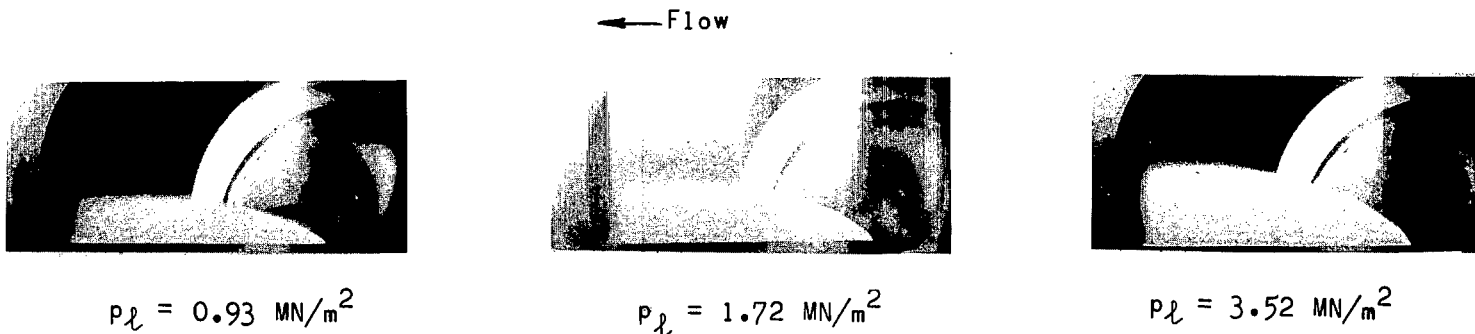
$$P_d = 3.52 \text{ MN/m}^2$$



(c)  $p_t = 6.89 \text{ MN/m}^2$ ; 3 orifices.

L-70-1607

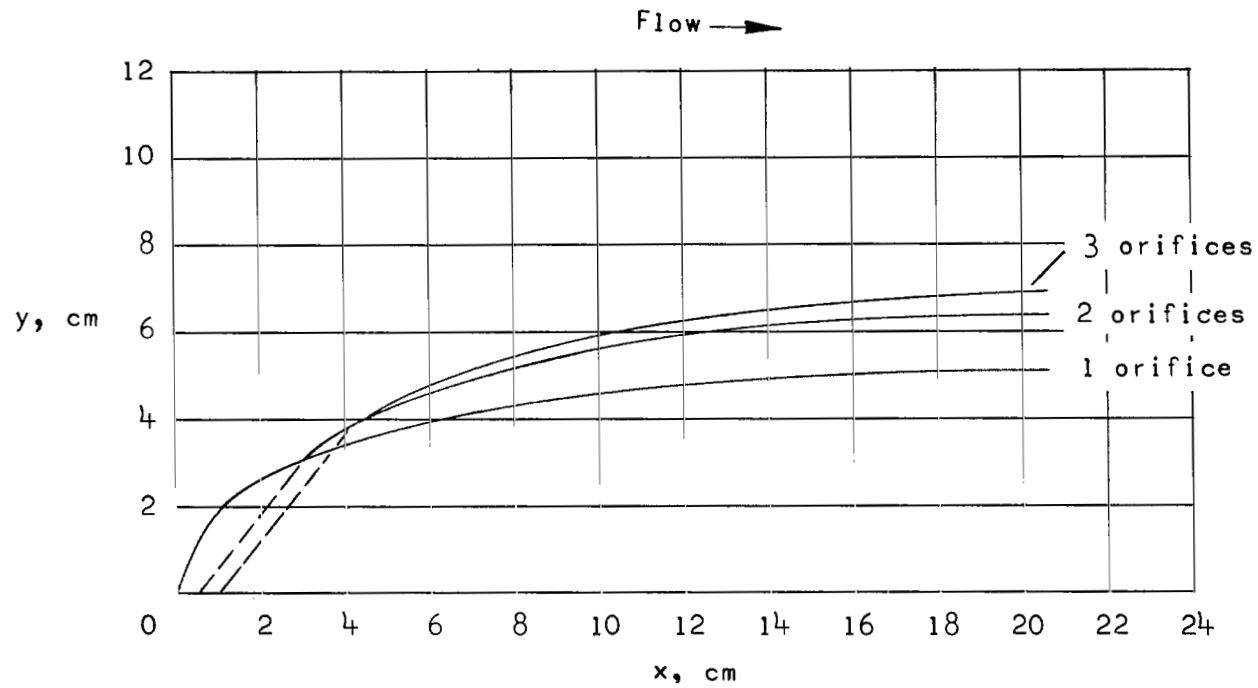
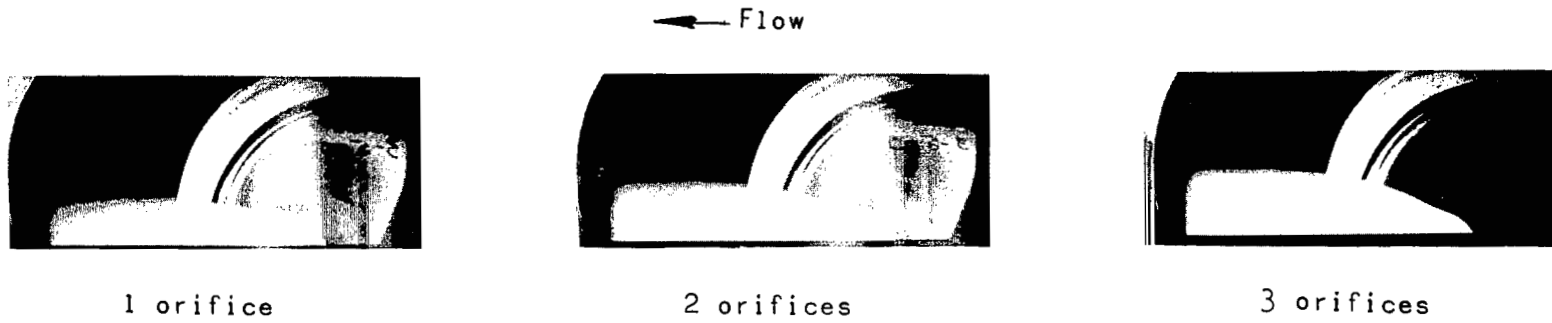
Figure 6.- Continued.



(d)  $p_t = 3.45 \text{ MN/m}^2$ ; 3 orifices.

L-70-1608

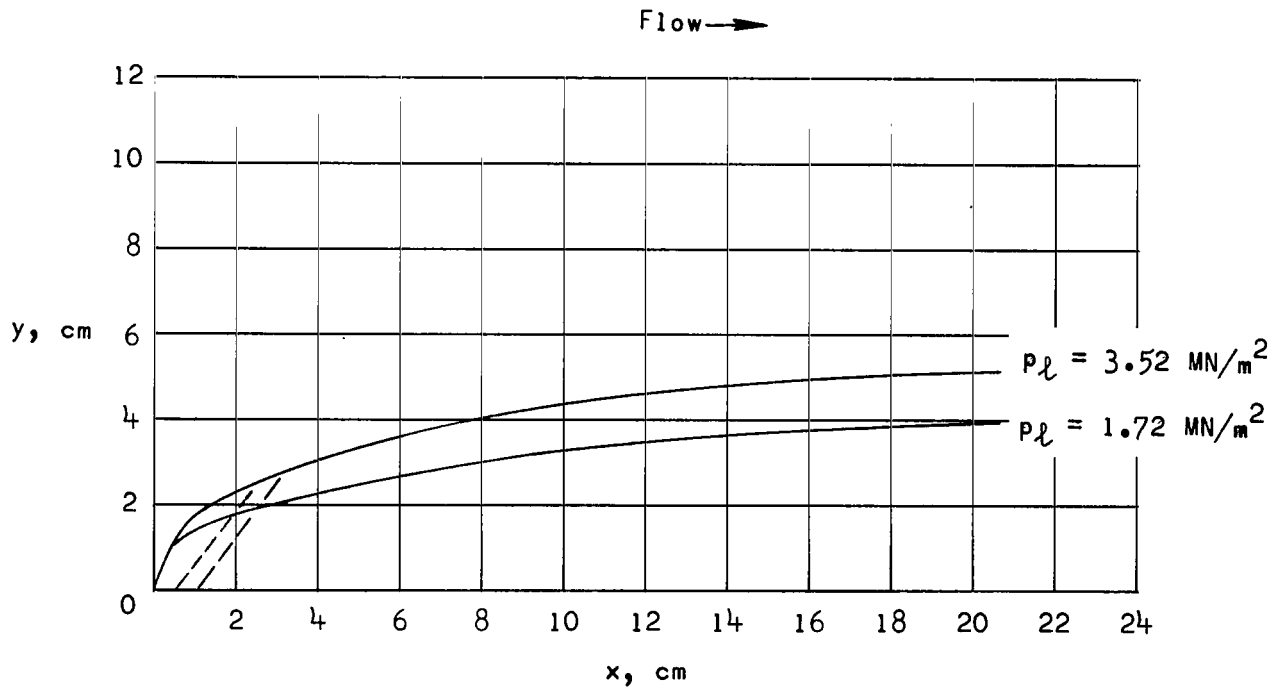
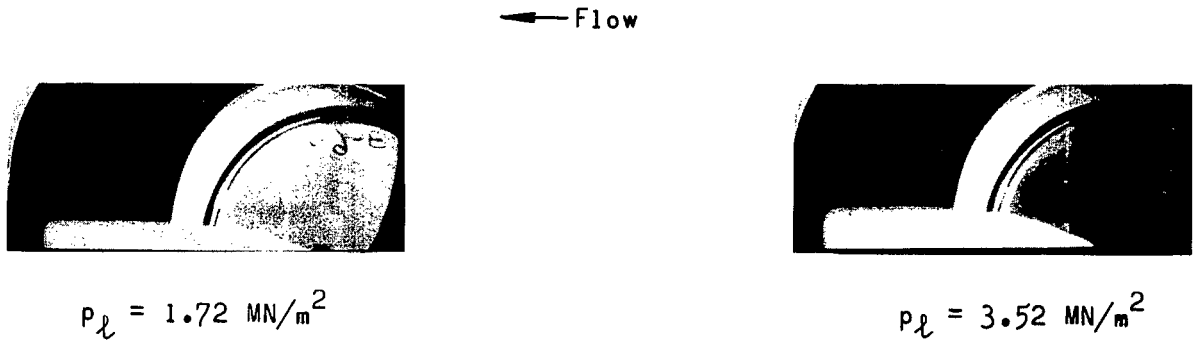
Figure 6.- Concluded.



(a)  $p_t = 3.52 \text{ MN/m}^2$ ;  $p_t = 6.89 \text{ MN/m}^2$ .

L-70-1609

Figure 7.- Light-screen photographs and measured outer limit of water spray trajectories for orifice configuration 3.



(b)  $P_t = 17.23 \text{ MN/m}^2$ ; 3 orifices.

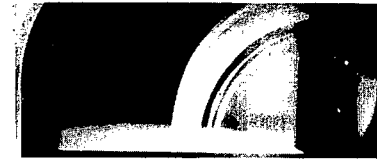
L-70-1610

Figure 7.- Continued.

← Flow



$p_l = 0.55 \text{ MN/m}^2$



$p_l = 0.93 \text{ MN/m}^2$

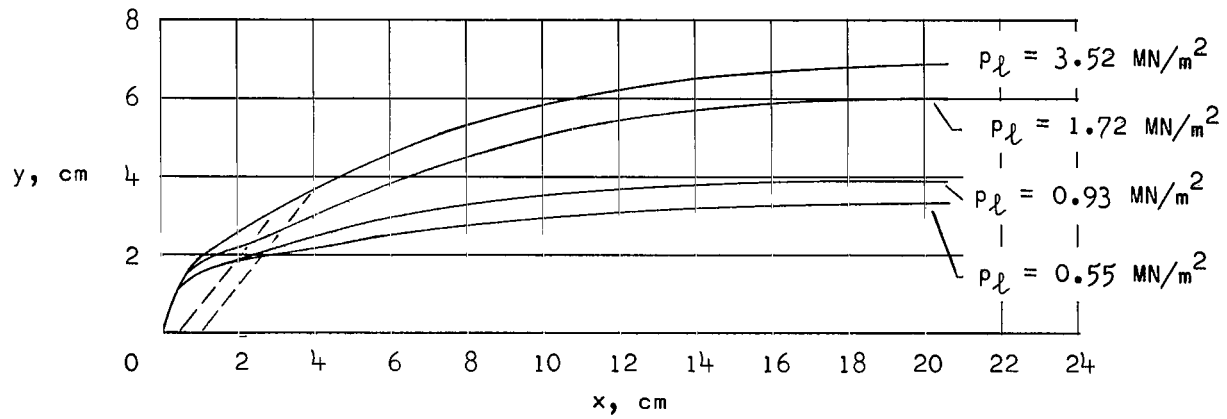


$p_l = 1.72 \text{ MN/m}^2$



$p_l = 3.52 \text{ MN/m}^2$

Flow →



(c)  $p_t = 6.89 \text{ MN/m}^2$ ; 3 orifices.

L-70-1611

Figure 7.- Continued.

← Flow



$$p_l = 0.55 \text{ MN/m}^2$$



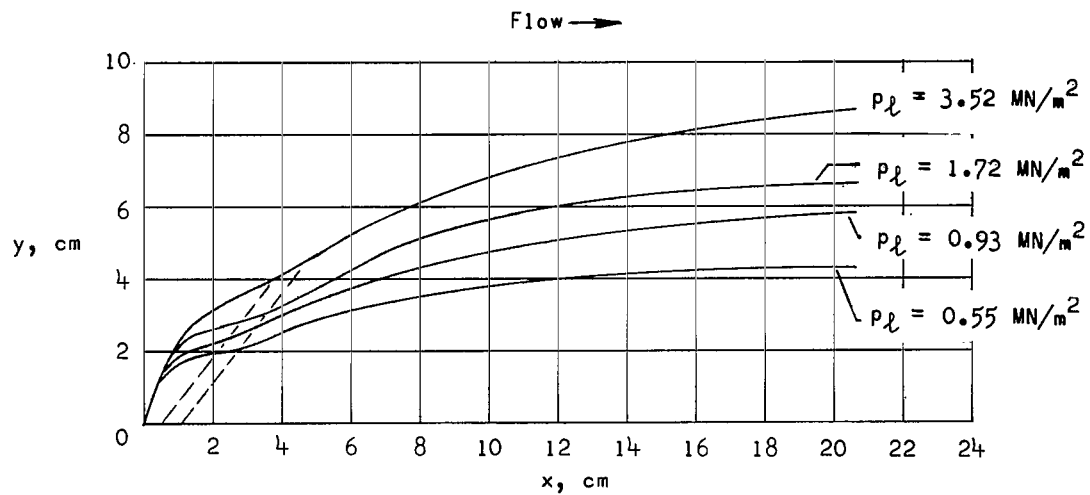
$$p_l = 0.93 \text{ MN/m}^2$$



$$p_l = 1.72 \text{ MN/m}^2$$



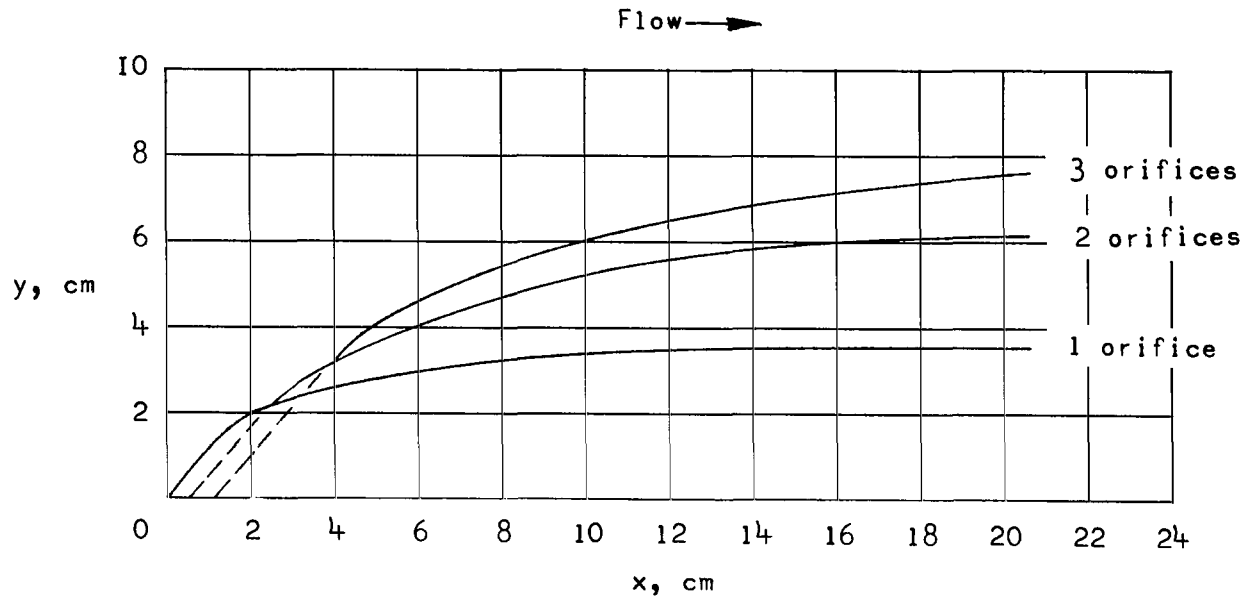
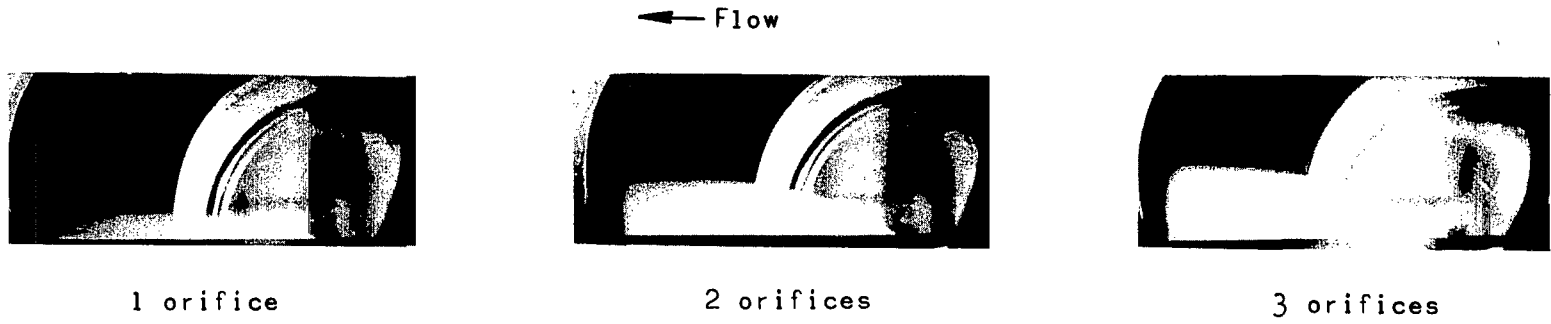
$$p_l = 3.52 \text{ MN/m}^2$$



(d)  $p_t = 3.45 \text{ MN/m}^2$ ; 3 orifices.

L-70-1612

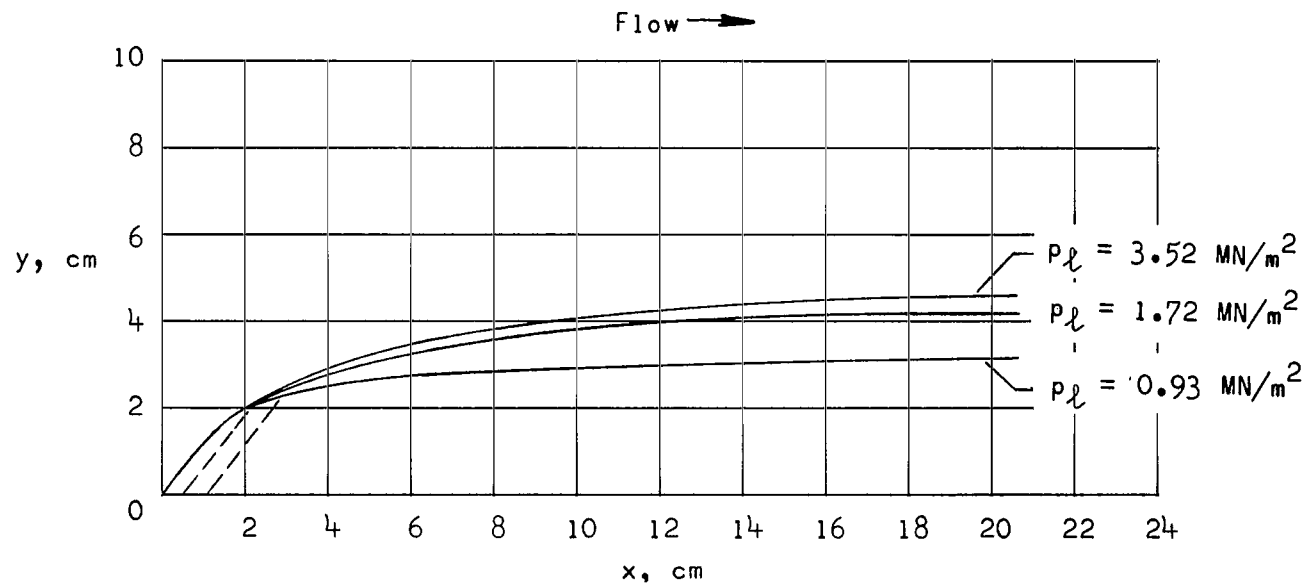
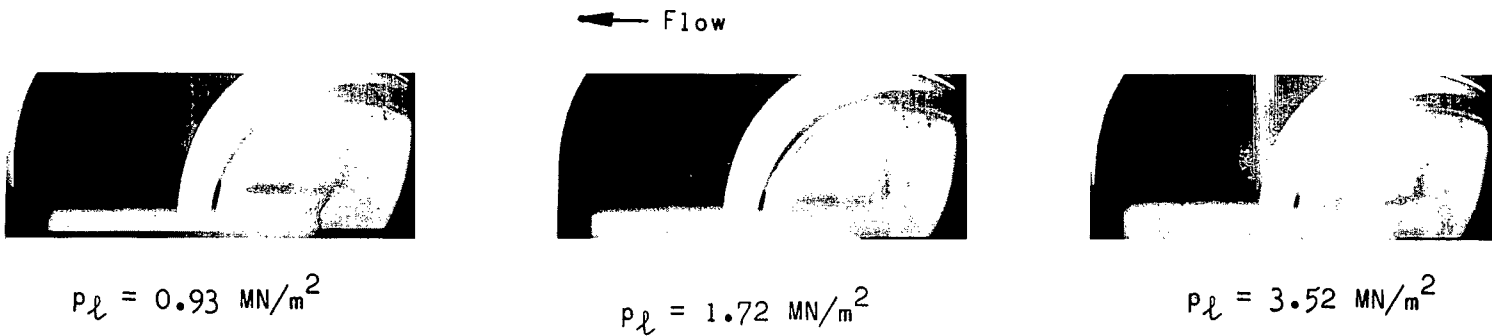
Figure 7.- Concluded.



(a)  $p_t = 3.52 \text{ MN/m}^2$ ;  $p_t = 6.89 \text{ MN/m}^2$ .

L-70-1613

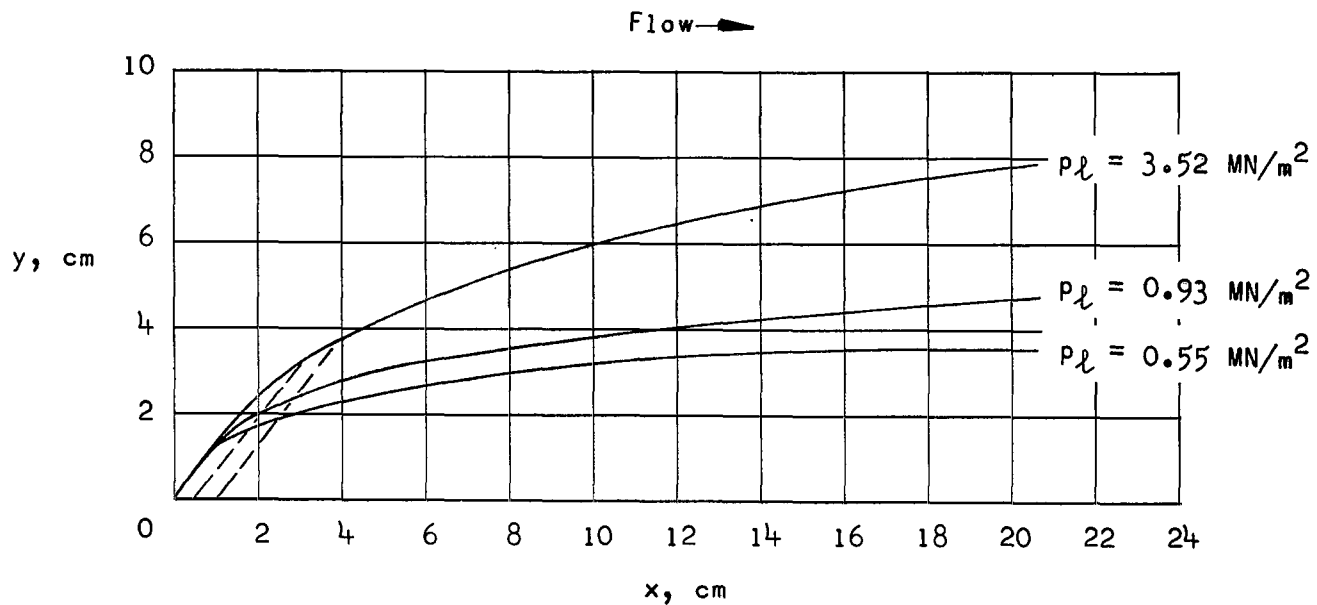
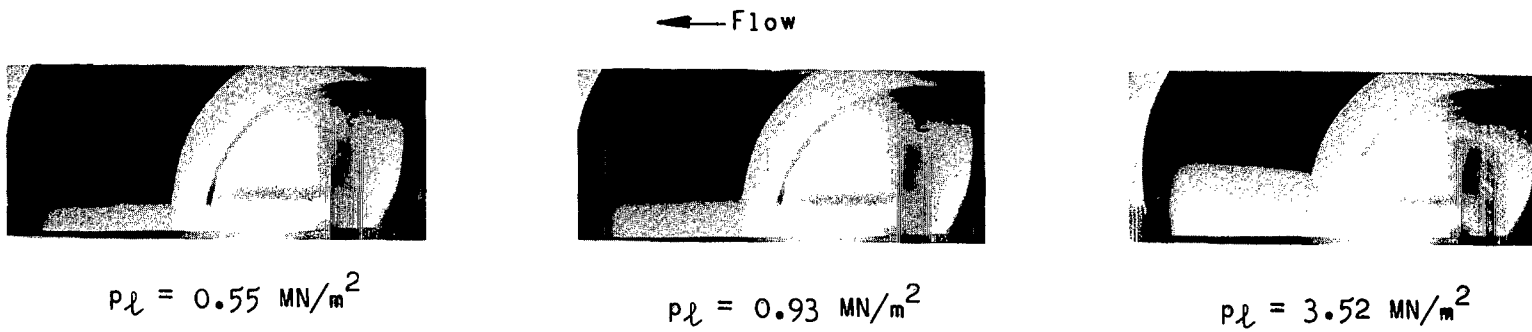
Figure 8.- Light-screen photographs and measured outer limit of water spray trajectories for orifice configuration 4.



(b)  $p_t = 17.23 \text{ MN/m}^2$ ; 3 orifices.

L-70-1614

Figure 8.- Continued.

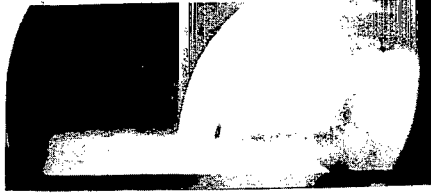


(c)  $p_t = 6.89 \text{ MN/m}^2$ ; 3 orifices.

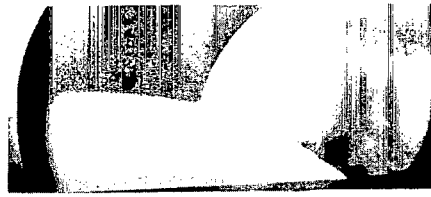
L-70-1615

Figure 8.- Continued.

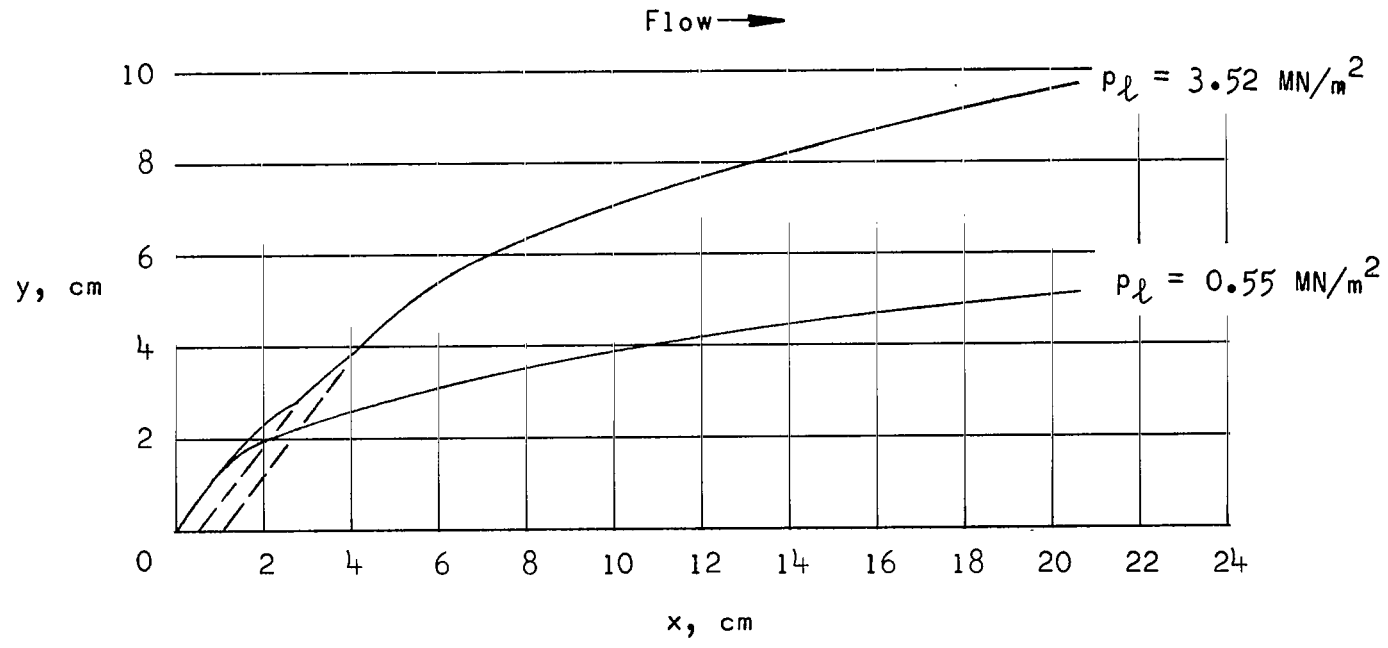
← Flow



$$p_l = 0.55 \text{ MN/m}^2$$



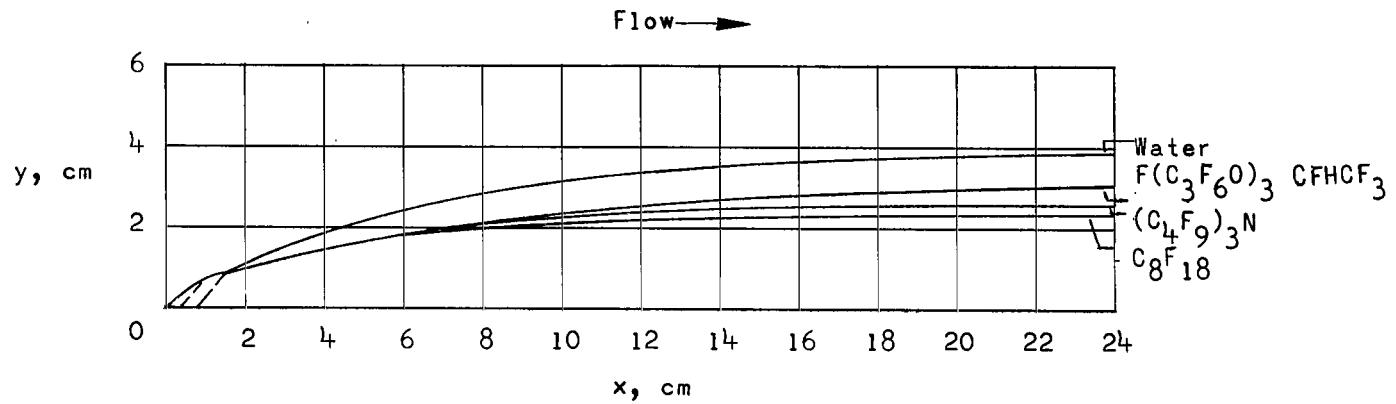
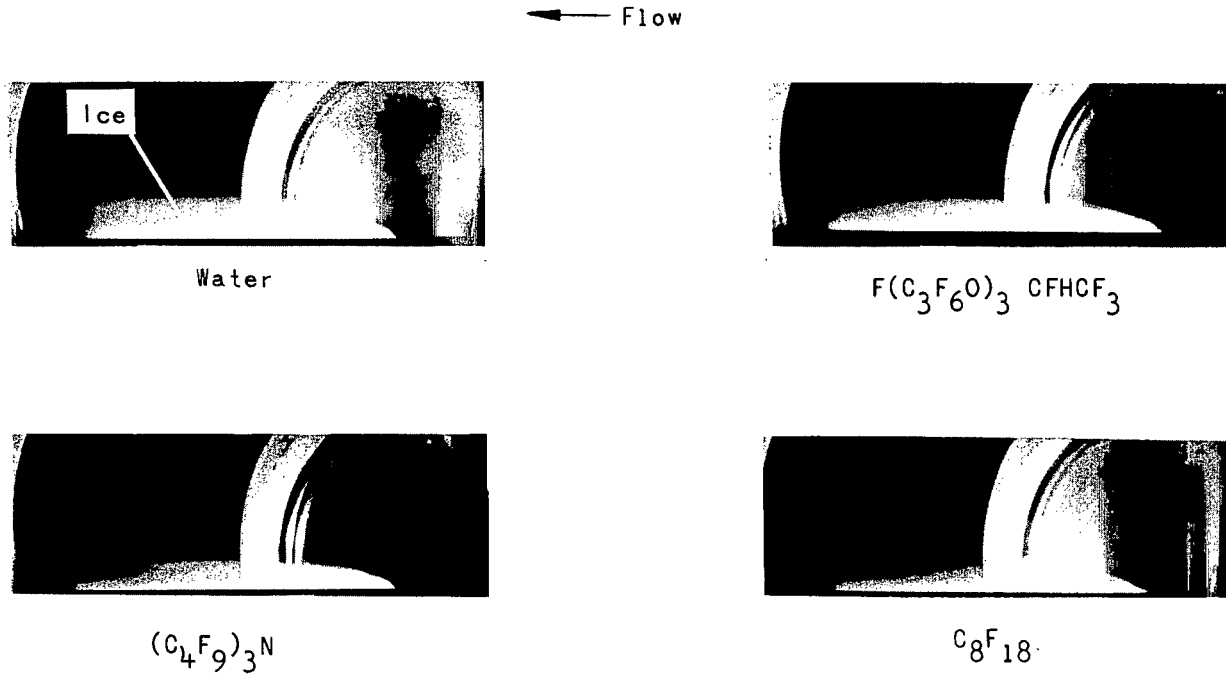
$$p_l = 3.52 \text{ MN/m}^2$$



(d)  $p_t = 3.45 \text{ MN/m}^2$ ; 3 orifices.

L-70-1616

Figure 8.- Concluded.



(a)  $p_t = 6.89 \text{ MN/m}^2$ .

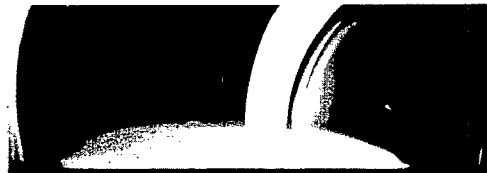
L-70-1617

Figure 9.- Light-screen photographs and measured outer limit of spray trajectories for injection of water and three formulations of fluorocarbon liquid. Fluid injection pressure was constant at  $0.48 \text{ MN/m}^2$ ; 3 orifices.

← Flow



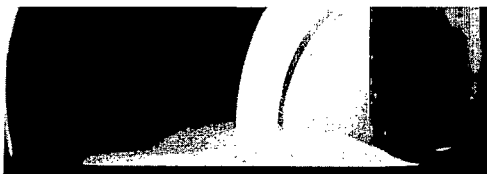
Water



$F(C_3F_6O)_3$   $CFHCF_3$

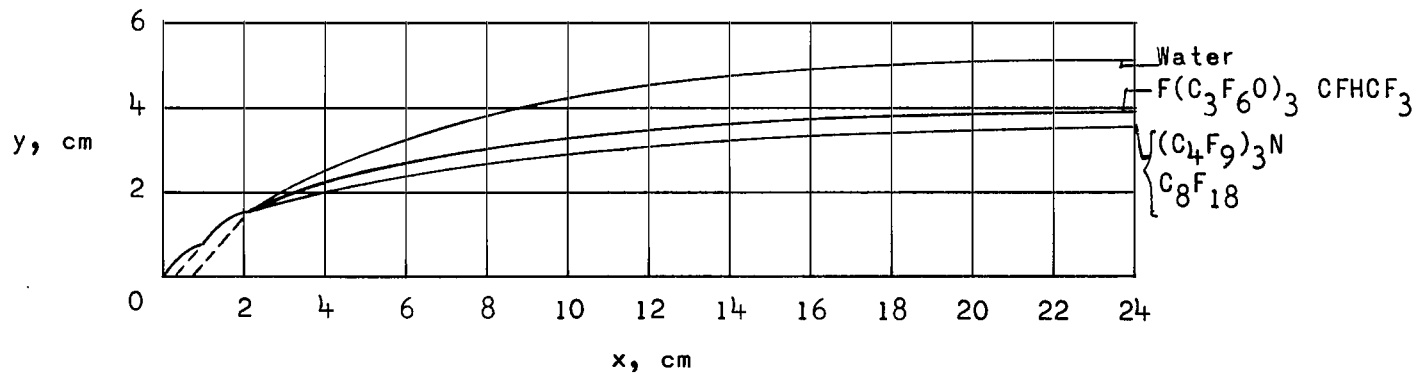


$(C_4F_9)_3N$



$C_8F_{18}$

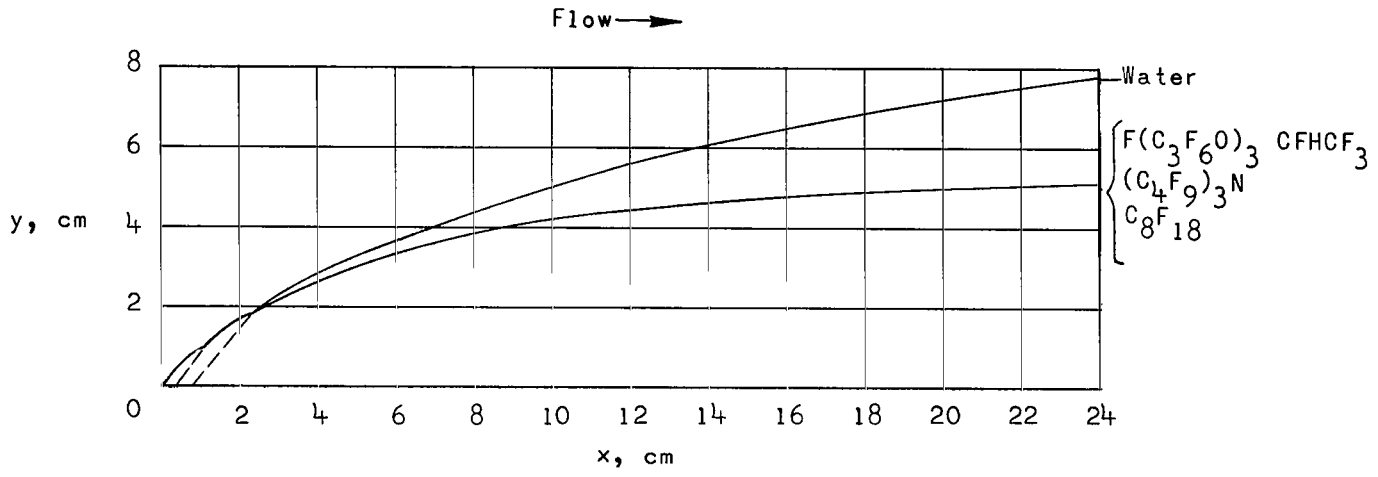
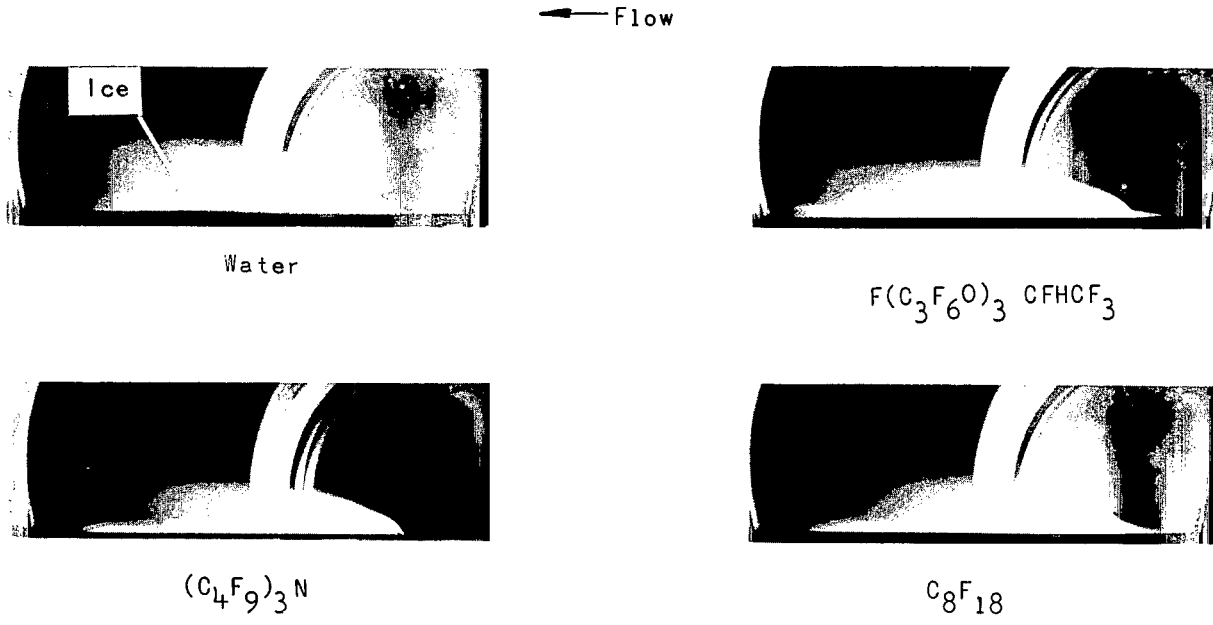
Flow →



(b)  $p_t = 3.45 \text{ MN/m}^2$ .

L-70-1618

Figure 9.- Continued.

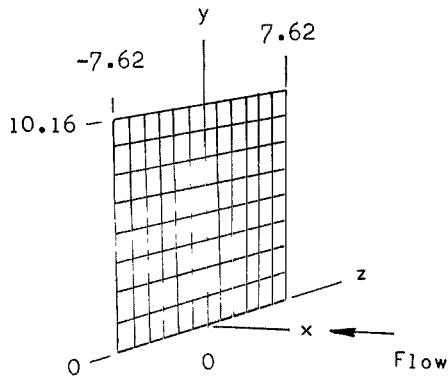


(c)  $p_t = 1.72 \text{ MN/m}^2$ .

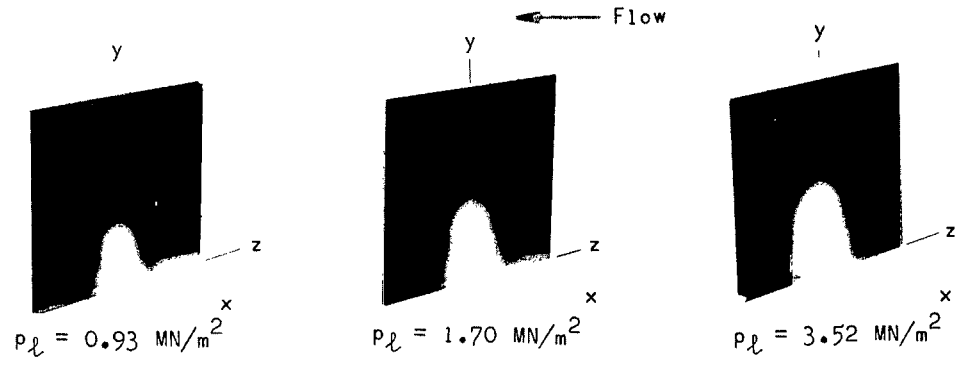
L-70-1619

Figure 9.- Concluded.

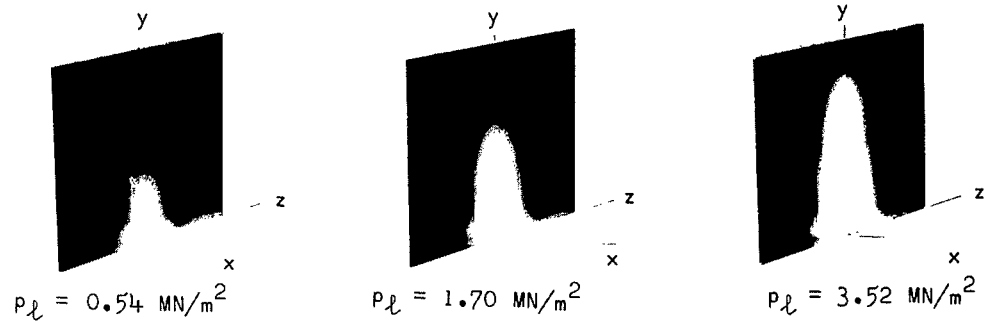




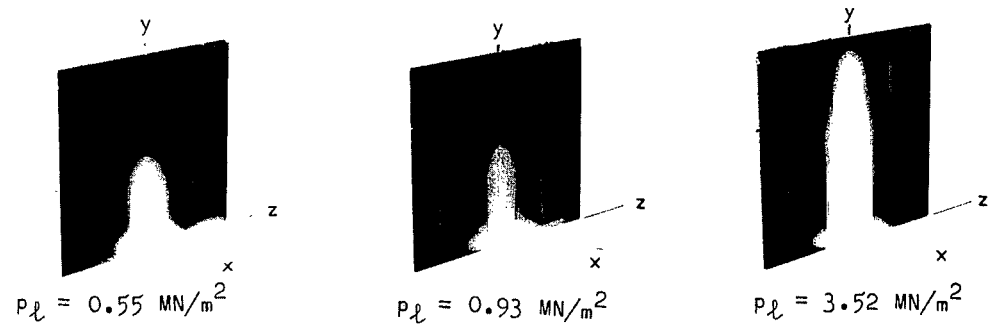
Grid scale, cm



(a)  $p_t = 17.23 \text{ MN/m}^2$ .



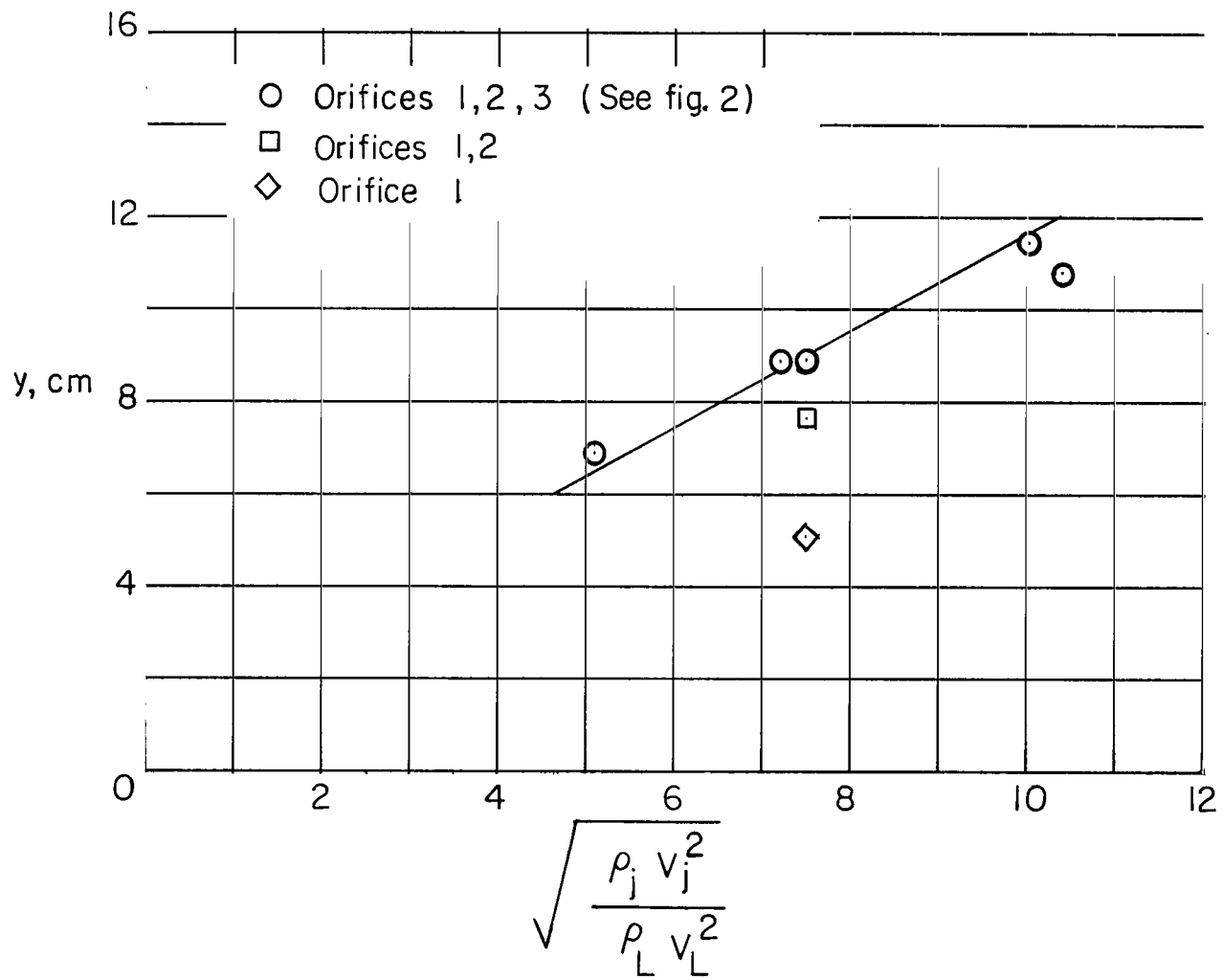
(b)  $p_t = 6.89 \text{ MN/m}^2$ .



(c)  $p_t = 3.45 \text{ MN/m}^2$ .

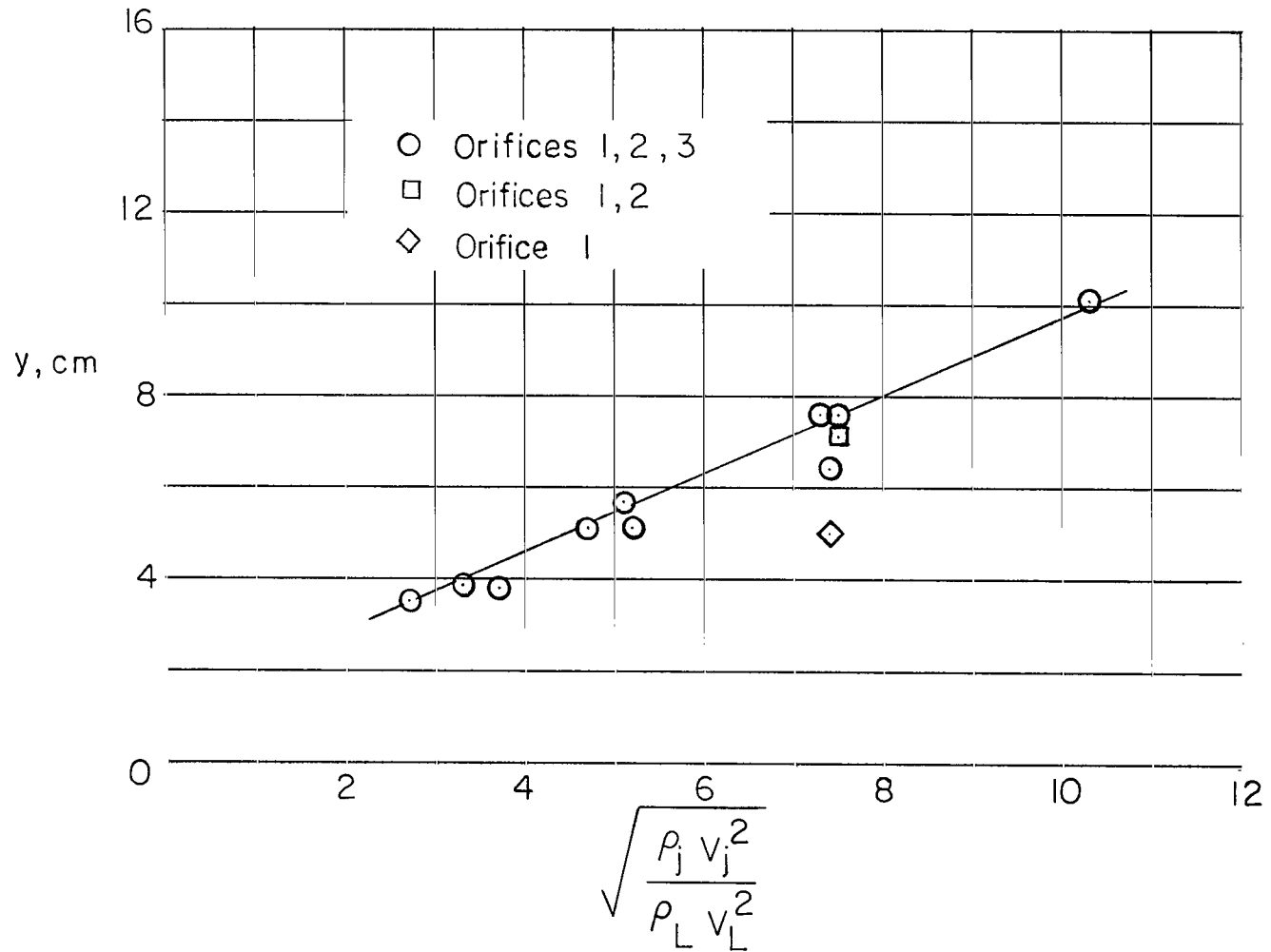
L-70-1621

Figure 11.- Spray cross-section photographs showing lateral spreading of liquid water approximately 16 cm from injection point for orifice configuration 4 (3 orifices).



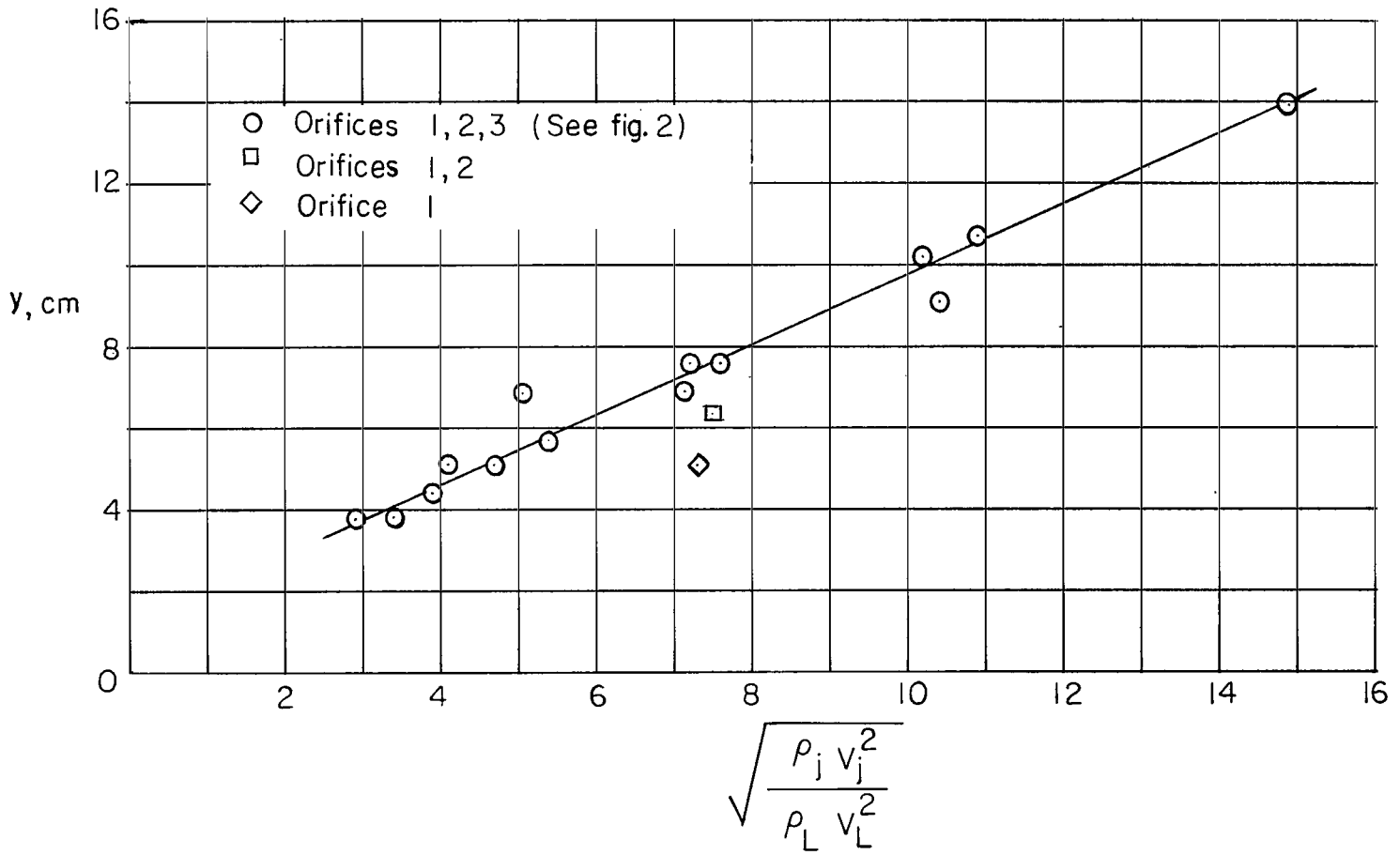
(a) Orifice configuration 1.

Figure 12.- Maximum spray penetration as a function of correlation parameter.



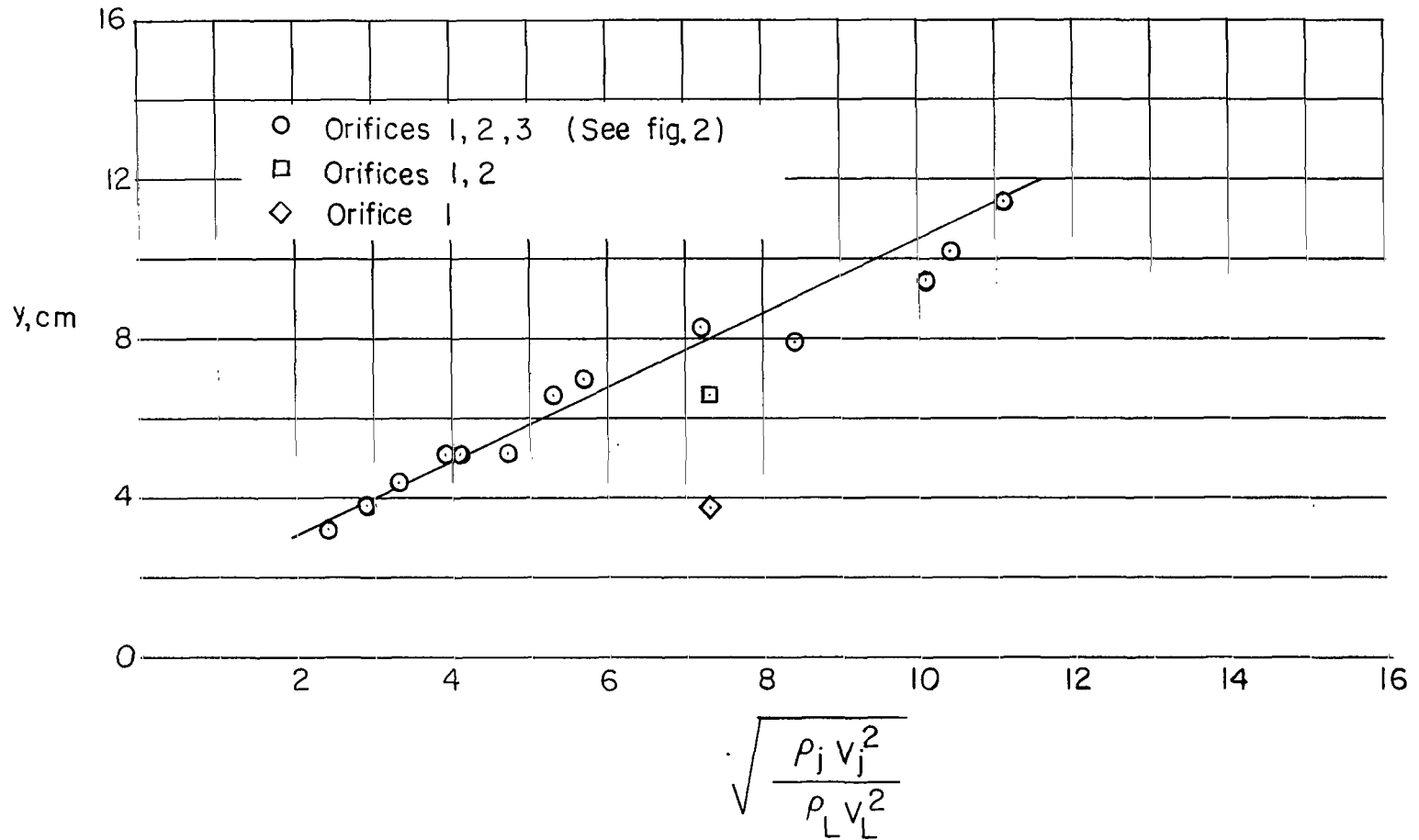
(b) Orifice configuration 2.

Figure 12.- Continued.



(c) Orifice configuration 3.

Figure 12.- Continued.



(d) Orifice configuration 4.

Figure 12.- Concluded.